Università degli Studi di Genova

Doctorate in

Sciences and Technologies of Chemistry and Materials

Curriculum: Materials Science and Technology

Structures and phase equilibria in the ternary Cu-As-Sb system

Marianne Mödlinger

Supervisor: Prof. Pietro Manfrinetti

Thesis defense: March 17, 2023

Table of content

1. Introduction: History and usage of Cu-As and Cu-Sb alloys 4

2. Aims and objectives 7

3. The Cu–As–Sb system: literature review 8

3.1 The As–Cu system 8

3.2 The As–Sb system 10

3.3 The Cu–Sb system 10

3.4 The Cu–As–Sb system 12

4. Methodology and experimental setup 13

4.1 Synthesis 13

4.2 Sample characterisation 18

4.2.1 Microstructure analyses (LOM) 18

4.2.2 Chemical analyses (SEM-EDXS) 18

4.2.3 Differential Thermal Analyses (DTA) 18

4.2.4 Differential Scanning Calorimetry (DSC) 19

4.2.5 X-Ray powder diffraction (XRD) 19

4.2.6 Single crystal X-ray diffraction (XRD) 19

4.2.7 Transport/physical property measurements 20

5. Results and discussion 22

5.1 Microstructure and chemical analyses (LOM and SEM-EDXS) 22

5.2 Differential Thermal Analyses (DTA) 30

5.3 Differential Scanning Calorimetry (DSC) 33

5.3.1 Cu_3As 33

5.3.2 Cu_5As_2 33

5.4 X-ray powder and single crystal diffraction (XRD) 34

5.4.1 Cu-As-Sb system 34

5.4.2 Cu-As system: Cu_3As 38

5.5 Transport/physical property measurements 43

5.5.1 $Cu_{9-x}(As,Sb)_3$: (sample C7) 43

5.5.2 Cu_3As 44

6. Conclusions and outlook 45

7. Acknowledgments 49

8. Publications 49

9. References 50

Structures and phase equilibria in the ternary Cu-As-Sb system

1. Introduction: History and usage of Cu-As and Cu-Sb alloys

Despite being the earliest produced alloy [1-2], the characteristics of **Cu-As alloys** are poorly understood. Cu-As alloys with low percentages of metals and metalloids such as Ni and Sb, are typically found in European prehistoric metal artifacts made from sulfosalt or fahlore minerals. After its early use in the late Neolithic/Early Bronze Age (~ 2300 BC) in Central Europe, Cu-As alloys were replaced by Cu-Sn alloys. Over 1/3rd of the European Copper and Bronze Age metal finds are Cu-As alloys with >1 wt.% As and all of them contain significant levels of Sb [3].

Some of the oldest, and certainly most impressive objects made of **Cu-As-Sb alloys** are known from the Nahal Mishmar hoard, Israel, which is dated to the earlier fourth millennium BC (Chalcolithic period) [4]. Some of the objects (and also contemporary objects from find spots from nearby, as Nahal Zeelim), most of them as-cast, contain up to 6 wt.% As and up to 22 wt.% Sb, which resulted in a unique, violet-pink colour. Similar compositions are known from ingots from the Middle and Late Bronze Age in Switzerland, few Late Bronze Age hoards in Slovenia, and a 6th century BC hoard at Arbedo, Ticino, Switzerland [5]. Since then, such alloy compositions are particularly rare in prehistory and basically unknown in history; today's usage of such alloys is unknown. Also, the synthesis of As-Cu-Sb alloys is so far only known from the Bronze Age [5].

Similar to Cu-As alloys, the origin of **Cu-Sb alloys** can be found in the Bronze Age. Sb decreases oxidation and, with growing amounts of Sb, Cu-Sb turn into a silvery-bluish colour and turns pink with growing amounts of Sb (Cu_2Sb), which likely was very attractive in prehistory [6]. As Cu-Sb alloys get brittle with increasing amounts of Sb, they were of little use for the production of tools and weapons but were used for the production of ritual items or

jewellery. Opposite to As, Sb was known in its pure form in prehistory; for instance, a tablet (TM.75.G.2154) from the archival resources from Ebla (3rd millennium BC) mentions roughly 19 kg of antimony paste for the manufacture of a jar. Early Bronze Age Antimony beads containing between 97-99.5 wt.% Sb are known from Tell Leinan (2500-2300 BC) and Jerablus Tahtani, Syria [7]. Further examples of early Cu-Sb alloy objects, but also some Cu-As-Sb alloy objects, are listed in [7].

Today, **Cu-As alloys** are of limited use in heat exchangers and condensers with fresh water; As is used in the gallium-arsenide semiconductor and microchip industry, in additives for lead car batteries, and in anti-friction agents for bearings [8-9] Unfortunately, As and Sb represent a high health risk for e-waste recycling workers [10-13].

Material properties of the **Cu-As system** between 1-8.6 at.% As (such as alloy's hardness, work-hardening, tensile strength, toughness, and brittleness) have been studied only by M. Mödlinger [1-2, 6, 14] and few archaeologists and scientists [15-24]. However, no data exist neither for mechanical, nor physical properties of any Cu-As alloy in combination with Sb impurities or Sb as alloying element.

While the investigation of **Cu-As and Cu-As-Sb alloys** is essential to archaeologists to better understand prehistoric metallurgy, at the same time their study is interesting also for other research fields:

- **extractive metallurgy**: The Cu-As system is of particular importance for extractive metallurgy as copper mined from sulfosalt minerals, such as tetrahedrite, tennantite, and enargite (all so-called Fahlores), which are characterized by high concentrations of arsenic (As) and antimony (Sb). Separating Cu from As and Sb is a heavily polluting process; a better understanding of the systems phases and correlated characteristics might lead to a less polluting process.
- **material science**: In material science, the research into Cu-As and Cu-As-Sb alloys is promising for discovering new potential technological applications, especially as there is no study yet carried out on the Cu-As-Sb system. Although the Cu-As binary phase diagram has been the subject of numerous investigations during the last century, it still lacks detailed studies; even more, most of it is reported with

uncertainty. Only few Cu-As compounds have been reported to form. However, neither the crystal structure (and so the true stoichiometry), nor the field of existence in the Cu-As-Sb system nor the physical properties have been determined for any of these compounds.

In addition to the lack of property studies for **Cu-As** based alloys, the situation is similar concerning corrosion studies [25-28]. While the binary Cu-As system has been evaluated [14, 22], the ternary phase diagram of the Cu-As-Sb system has not yet been studied at all. The lack of scientific research into parent Cu-As alloys and those containing more than 0.85 at.% As is somewhat surprising given that Cu-As alloys exhibit a host of interesting and beneficial characteristics, such as:

- As prevents porosity in Cu, even when cast under oxidizing conditions (ideal for works requiring welding/brazing);
- As reduces the crystalline structure in castings, which may result in increased tensile strength. With the addition of up to 1 wt.% arsenic, a solid solution forms that has slightly increased tensile strength while maintaining ductility;
- Cu-As alloys are highly ductile up to 15.7 at.% As [17];
- Cu-As alloys show high corrosion resistance: Arsenic prevents dezincification and imparts the resistance of stress corrosion cracking in brasses [8, 29-30]; shows inhibitory effects on admiralty and aluminium brasses [31]; studies of archaeological tin (Sn) bronzes have shown that areas rich in As and Sb along grain boundaries are immune to bacteria-induced corrosion, as demonstrated by M. Mödlinger and others [32-33]. In 3,000 year old Cu-As objects a stable γ-phase often precipitates on the surface and at the grain boundaries.

Most recently, the **Cu-Sb system** was determined experimentally extensively by Fürtauer and Flandorfer [34]. Today, this binary alloy is of high interest as a base for ternary and quaternary lead-free high-temperature soft solders (melting range: 230-350°C) [34].

2. Aims and objectives

The PhD focuses on the determination of the ternary Cu-As-Sb phase diagram in the copper-rich corner of the system (64-100 at.% Cu). There are no works carried out on the Cu-As-Sb system yet; only the respective binary systems were studied [22-23, 34-37].

After starting the experimental work on the ternary Cu-As-Sb system, it became soon clear that the planned analyses would not have provided sufficient insight into the study of this system: it was quickly noted that some of the data reported for the Cu-As diagram was unreliable and the system was still lacking fundamental data that was and is essential for the interpretation of results from the work on the ternary Cu-As-Sb system. Consequently, it has been decided to study formation, crystal structure and polymorphism of intermetallics of the Cu-As system (mostly Cu_3As and Cu_5As_2; both reported dimorphic, each one with a low- and high-temperature structure). Moreover, it was also planned to perform further and deeper analyses as crystal structure determinations and physical properties measurements.

It is the aim of the PhD-research to investigate the ternary phase diagram by:

- **Studying** the alloys in as-cast and annealed condition to understand phase formation and phase stability, the crystallo-chemical characteristics and structural transitions;
- **Determining** the copper-rich corner of the Cu-As-Sb phase diagram (64-100 at.% Cu);
- **Identifing** new phases and ternary compounds yet unknown, study their thermodynamic stability and crystal structure(s);
- **Planning** (future) specific physical properties measurements, in view of identifying desirable and exploitable properties of either the binary or ternary compounds.

3. The Cu–As–Sb system: literature review

3.1 The As–Cu system

The last assessment of the As–Cu system was carried out by Subramanian – Laughlin [22-23] and is based on several decades of research by a variety of different researchers. The investigation of the phase diagram above circa 46. at.% As is still missing due to the high oxidation rate of As. Four intermediate phases are reported (**Figure 1**):

- **α** with a maximum solubility of 6.83 at.% As in the Cu matrix;
- **β** (unclear stoichiometry: reported as either Cu_9As, Cu_8As, or Cu_6As; 11.1-14.3 at.% As; *cph* Mg-type structure). β forms by a peritectic reaction at 325±25°C;
- **γ** (Cu_3As) has been confirmed to have a range of homogeneity independent from the temperature. γ forms from the liquid through a congruent reaction at 827°C. It is separated into two hexagonal polymorphs (which were not confirmed during our research, see **section 5.4.2**, identifying Cu_3As as of Cu_3P-type, *hP*24, Space group: P63cm (no. 185)):
  - **HT** (high temperature) **γ** at 450-475°C (Pearson symbol: *h*P8; Space group *P*63/*mmc*; DO_{18}; prototype: Na_3As) and a
  - **LT** (low temperature) **γ'** at <450°C (Pearson symbol: *hP*24; Space group: *P*–3*c*l/---; prototype: Cu_3As).

The formation of a Cu_3As phase as **cubic α-domeykite** has been reported by Koenig [39] by passing As-vapour over Cu at 500°C and by Weil [40] at ordinary pressures. Pearson assigns α-domeykite with the space group I-43d [41]; this constitutes the only study on α-domeykite, relaying on single crystal measurements on one natural crystal only. High-pressure synthesis of cubic Cu_3As was reported by Bolfa et al. [42] and dissociates into hexagonal Cu_3As and Cu_8As on heating to 225°C. Cubic α-domeykite is known from archaeological Cu-As bronzes [1]. **β-domeykite** has a hexagonal structure that was found to correspond crystallographically to the equilibrium γ-phase (or Cu_3As), and, consequently, to the Pearson symbol *hP*24 and space group *P*–3*c* [43]. It is also reported in nature as mineral domeykite.

Research carried out during this PhD research though showed that Cu_3As crystallises in the hexagonal Cu_3P-type (*hP*24, *P*63*cm*, No. 185) and not the hexagonal anti HoH_3-type

[41]. Moreover, we also find that Cu_3As does not exist with other modifications at least up to 750 °C.

- **δ** (given with the possible stoichiometries Cu_5As_2, $Cu_{9.5}As_4$, and $Cu_{19}As_8$; ~29 at.% As;) forms by a peritectic reaction at 709°C and is present in the following polymorphs:
  - **HT δ** (Pearson symbol: *cF*16, space group *Fm*3*m*; *D0*3; prototype: BiF_3) and a
  - **LT δ'** phase (Pearson symbol: *oI*28, space group *Ibam*; prototype: Cu_5As_2).

  The peritectic melting temperature of Cu_5As_2 is about 710°C. The HT δ is stable from the peritectic melting temperature down to 395°C, while the LT δ' is stable down to 300-315°C. The allotropic transformation of HT δ occurs at 380°C.

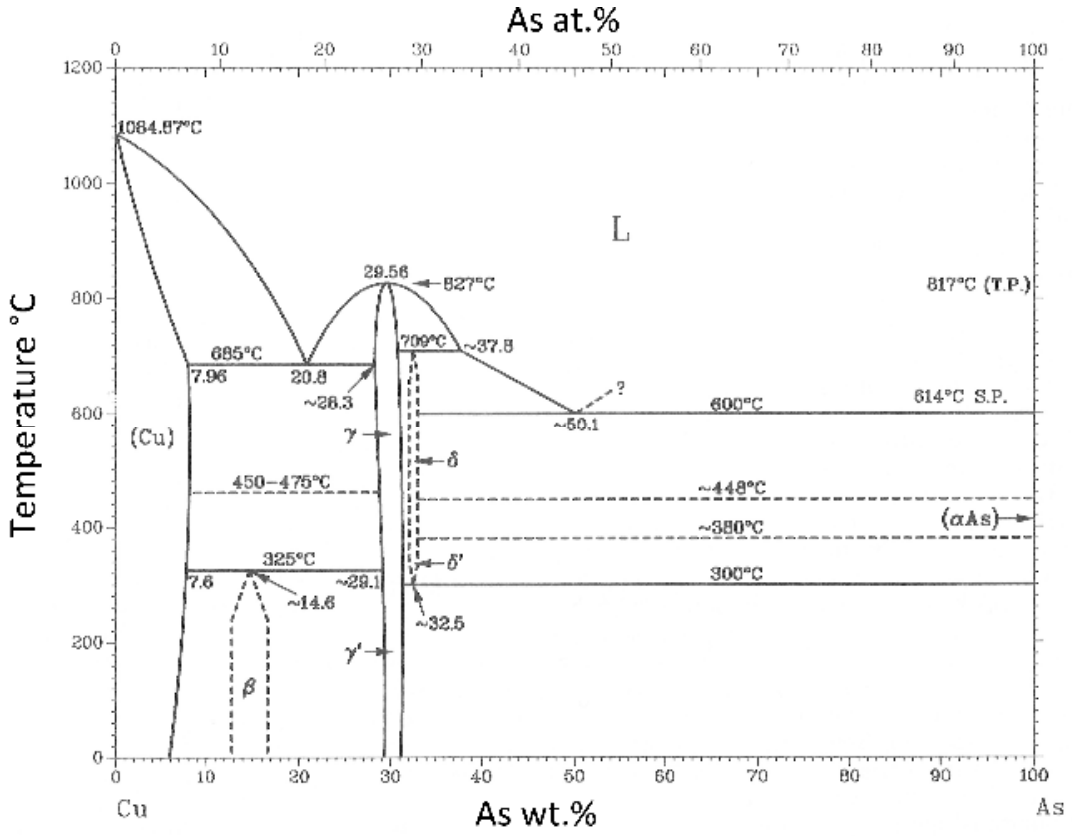

Figure 1. The binary As-Cu system [22]

A **metastable phase Cu_2As** identical to the naturally occurring mineral koutekite (space group: *P*4/*nmm* O2; prototype: Cu_2Sb). Cu_2As decomposes to Cu_5As_2 and (As) on heating to 179°C. This phase is not reported in the current phase diagram assessed [22-23].

Other **minerals** of the Cu-As system besides domeykite are: Algodonite (hexagonal Cu_7As, Cu_6As, or Cu_4As; decomposes when heated to Cu + Cu_3As at about 250°C), Whitneyite

(a mixture of algodonite and Cu, likely also metastable), and Paxite (metastable orthorhombic Cu_2As_3) [22-23].

3.2 The As–Sb system

A short assessment of the As–Sb system was carried out by Massalski [35], based on works of Hansen; Goncharov et al.; Ugai et al., [37] as well as older literature from 1912 to 1938. A miscibility gap in the solid state was not yet located but supported by a positive mixing enthalpy. Data on eventually present As-Sb phases, such As_3Sb_7, are yet completely missing **(Figure 2**).

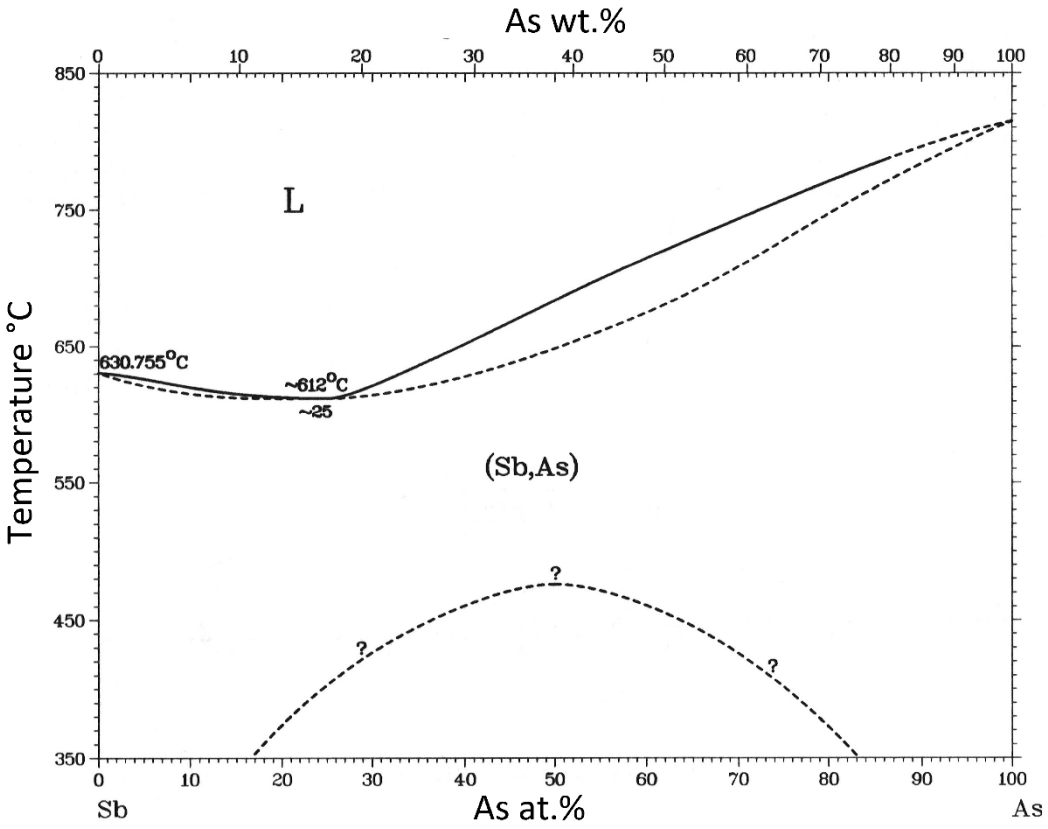

Figure 2. The binary As-Sb system [35]

3.3 The Cu–Sb system

The Cu–Sb system was assessed by Massalski; this assessment was recently updated by Fürtauer and Flandorfer, and Gierlotka – Jendrzejczyk-Handzlik (thermodynamics) [34, 36, 44] The following data is taken from [34]. From the Cu–Sb system six intermetallic phases are reported (**Figure 3**):

- **α (Cu)**: the maximum solubility of Sb in Cu is at 7.8 at.% at 645°C, 6.5 at.% at 484°C and 5.7 at.% at 440°C.
- **HT β** Cu_3Sb at 15.4-27.5 at.% (19.4-30.8 wt.%); or melts congruently at 690°C and crystallizes in a cubic BiF_3-type structure (DO3) with the space group *Fm*–3*m*. The phase decomposes in an eutectoid reaction at 427°C into ε and η.
- **γ** (Cu_4Sb) crystallizes in a Mg-type structure (Pearson symbol: hP2; space group: $P6_3/mmc$) and forms from (Cu) and β in a peritectoid reaction at 484°C.
- **δ** ($Cu_{78}Sb_{20}$) crystallizes in a $Cu_{78}Sb_{21}$ structure (Pearson symbol: *hP*98; space group: $P6_3/mmc$); the phase forms in a peritectoid reaction β+γ at 467°C.
- **ε** (Cu_3Sb) crystallizes in a Cu_3Ti structure (Pearson symbol: *oP*8; space group: *Pmmn*); the phase forms at 440°C in a peritectoid reaction from β+δ and transforms in an eutectoid reaction at 360°C to ζ+η.
- **ζ** ($Cu_{10}Sb_3$) crystallizes in a $Cu_{10}Sb_3$ structure (Pearson symbol: *hP*26; space group: *P*–3) and forms in a peritectoid reaction at 390°C (?) from δ+ε.
- **η** (Cu_2Sb) crystallizes in a Cu_2Sb structure (Pearson symbol: *tP*6; space group: *P*4*/nmm*); the Sb-rich β forms at 586°C at the liquid melt in a peritectic reaction the η-phase.

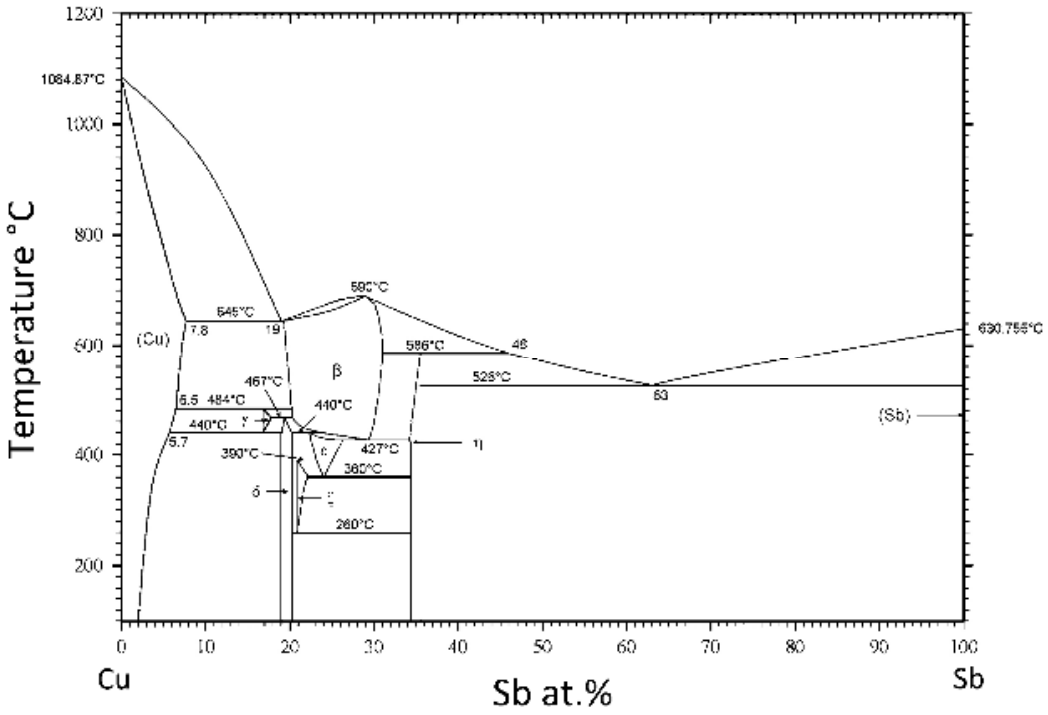

Figure 3. The binary Cu-Sb system [34]

3.4 The Cu–As–Sb system

There are no experimental studies available, and neither is any thermodynamic modelling of the Cu–As–Sb system. The herewith presented results for the Cu-rich corner are the first for this system.

4. Methodology and experimental setup

4.1 Synthesis

The metals used as starting materials were Cu 99.997 wt.% purity (MB: Metallwerke Brixlegg, Austria, MB-OF101 certified), arsenic lump 99.99 wt.% purity (Alfa Aesar), and antimony polycrystals 99.999 wt.% purity (Koch Light Laboratories LTD).

Cu and Sb pieces and As lumps, weighed in adequate stoichiometric amount, were sealed inside a quartz tube under vacuum and heated slowly (in steps of 40°C above 250°C) in an electric furnace until the desired temperature was reached. The samples were prepared at several temperatures between 300°C and 750°C.

In order to remove traces of oxides, before using, Cu pieces were treated in nitric acid (5-10 %), then rinsed with water and finally in absolute ethanol. For the same purpose, As lumps were sealed under vacuum in a Pyrex tube and then heated up to 300°C while keeping the top end of the tube right outside the furnace entrance; this treatment allowed As_2O_3 vapours to migrate towards and finally condense to the far cold end of the tube.

Of each alloy composition, about 10-15 g samples were prepared. The weighted elements were placed in a quartz tubes, sealed under vacuum and heated slowly (at steps of 40°C when above 250°C) in electric furnaces until molten (610-1100°C). Moving (shaking) the alloys before and once molten, favoured the reaction and decreased segregation phenomena. The maximum heating temperature was different for every sample; it was established through continuous observations of the sample heated up to the liquid. At this step, the sample was heated about 50°C higher. Finally, the alloys were quenched at room temperature while being moved inside the quartz tube. The alloys were left inside the quartz tube until analyses were carried out in order to prevent oxidation, which was common especially of As-rich samples (Group A) (**Figure 4**). Different parts of each alloy were then prepared for further analyses; such as: microstructural analyses, SEM-EDXS, XRD and DTA. The 31 parent alloys synthesized are listed in **Table 1**. The alloys were prepared in three groups with arsenic and antimony in different ratios: Group Cu-A (A=As_3Sb); Group Cu-B (B=AsSb) and Group Cu-C (C=$AsSb_3$) (**Figure 5**).

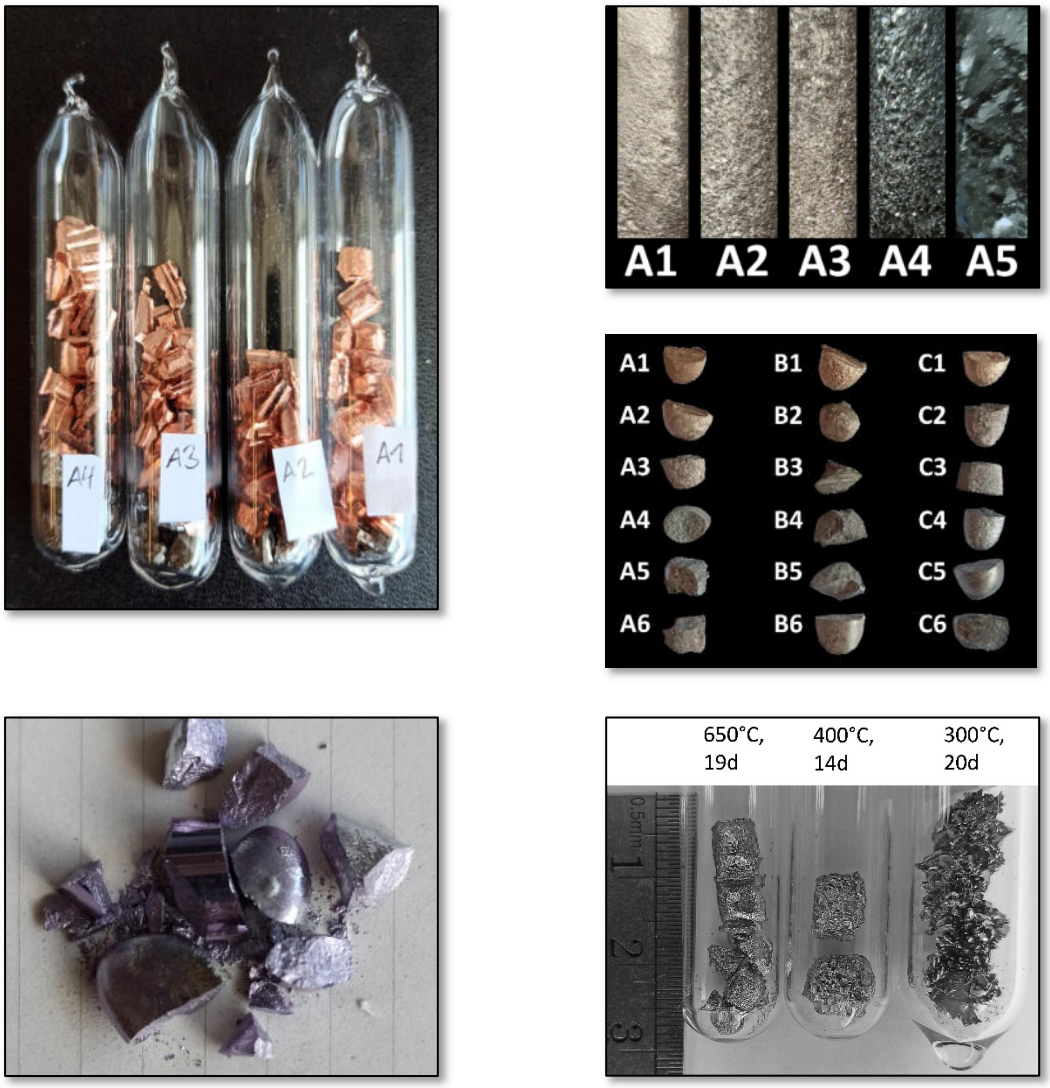

Figure 4. Synthesis. **Top left**: Quartz tubes with pure Cu, As and Sb in varying quantities. **Top right**: the first as-cast samples of Group A. **Centre right**: samples prepared for annealing at 500°C for 42 days. **Below left**: The particular colour of *tP*6 (as noted also for Cu_2Sb) is worth noting: different shades of violet and pink are easily recognisable (sample C8, $Cu_{68}As_8Sb_{24}$). **Below right**: Cu_3As samples prepared at different temperatures; note the difference in the formation of crystals.

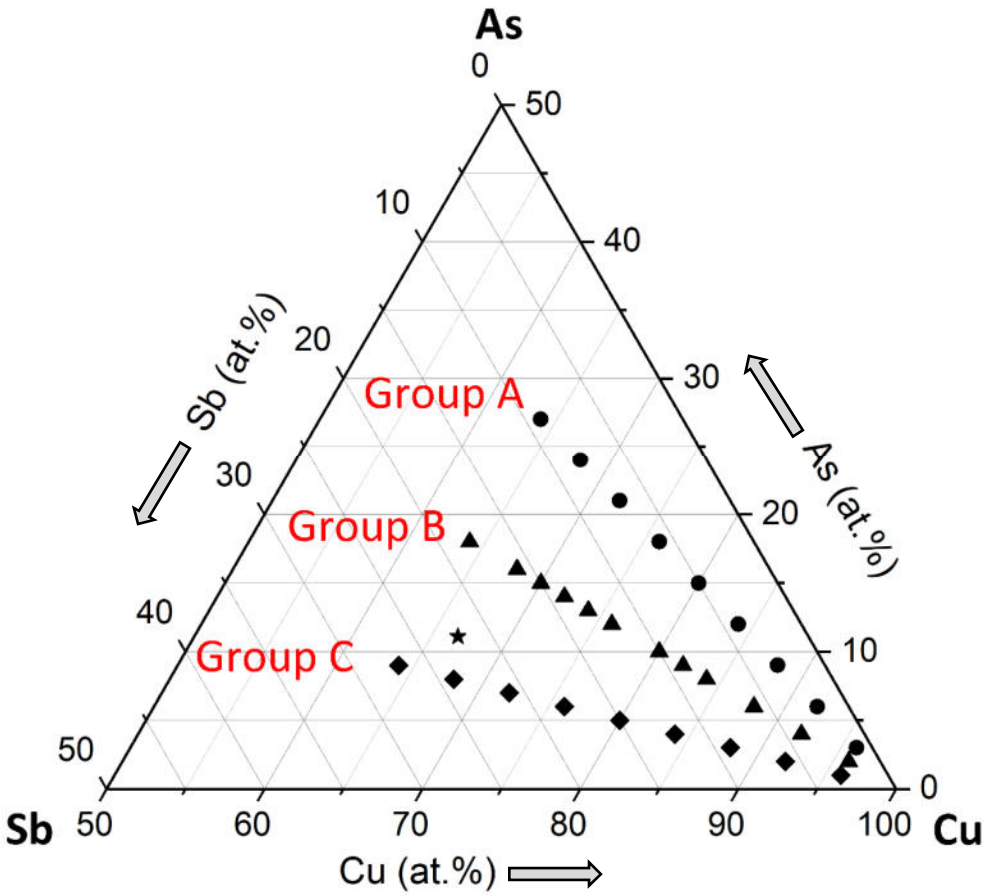

Figure 5. Alloys prepared in the Cu-As-Sb system.

Additionally to alloys of Groups A, B and C, we also aimed to prepare a sample for EDXS calibration standard with the composition of $Cu_2(As,Sb)$ (ratio 2:1; sample S2:1). However, such a single phase material was not obtained. Samples of these 31 parent alloys were studied in as-cast condition, after being subjected to DTA, and after several annealed treatments, resulting in a total of over 200 specimens for further analyses.

Thermal treatments (annealing/homogenization) were carried out on samples 1-6 from all three groups at 500°C and 600°C, respectively, for 42 days. Only the later DTA-analyses showed that the 600°C annealing was not significantly contributing to the understanding of phase formation for all phases, as around 600°C eutectic transformation also takes place. Further thermal treatment was carried out on samples A7 and B7 (450°C and 550°C for 30 days), as well as samples A5-6, B5-6 and C5-6 (300°C and 350°C respectively) and many more on binary samples (**Table 2**). **Table 3** provides an overview of further analyses carried out on selected samples.

Table 1. Overview on ternary alloys prepared, their thermal treatment and analyses carried out (x).

group	name	alloy	thermal treatment			DTA	Microstr. analyses			powder XRD			SEM-EDXS
			500°C	600°C	varia	as-cast	DTA	as-cast	500°C	600°C	DTA	as-cast	thermal treatment	
Cu-A (A=As_3Sb)	A1	$Cu_{96}As_3Sb_1$	x	x	-	x	-	x	x	x	-	-	-	500°C
	A2	$Cu_{92}As_6Sb_2$	x	x	-	x	-	x	x	x	-	-	-	500°C
	A3	$Cu_{88}As_9Sb_3$	x	x	-	x	-	x	x	x	-	-	-	500°C
	A4	$Cu_{84}As_{12}Sb_4$	x	x	-	x	x	x	x	x	x	-	-	DTA, 500°C, as-cast
	A5	$Cu_{80}As_{15}Sb_5$	x	x	300	x	x	x	x	x	x	x	300/7d; 500/42d; 600/42d	DTA, 500°C
	A6	$Cu_{76}As_{18}Sb_6$	x	x	300	x	x	x	x	x	x	x	300/7d; 500/42d; 600/42d	DTA, 500°C
	A7	$Cu_{72}As_{21}Sb_7$	-	-	450, 550	x	x	x	-	-	x	x	450 & 550/30d	DTA, as-cast, 450°C, 550°C
	A8	$Cu_{68}As_{24}Sb_8$	-	-	-	x	x	x	-	-	x	-	-	DTA, as-cast
	A9	$Cu_{64}As_{27}Sb_9$	-	-	-	x	x	x	-	-	x	x	-	DTA, as-cast
Cu-B (B=AsSb)	B1	$Cu_{96}As_2Sb_2$	x	x	-	x	-	x	x	x	-	-	500/42d	500°C
	B2	$Cu_{92}As_4Sb_4$	x	x	-	x	-	x	x	x	-	-	-	500°C
	B3	$Cu_{88}As_6Sb_6$	x	x	-	x	-	x	x	x	-	-	-	500°C
	B4	$Cu_{84}As_8Sb_8$	x	x	-	x	x	x	x	x	-	-	500/42d	DTA, 500°C, as-cast
	B4.5	$Cu_{82}As_9Sb_9$	-	-	-	x	-	x	-	-	-	-	-	-
	B5	$Cu_{80}As_{10}Sb_{10}$	x	x	350	x	-	x	x	x	-	-	350/18d; 500/42d	500°C
	B6	$Cu_{76}As_{12}Sb_{12}$	x	x	350	x	x	x	x	x	-	-	350/18d; 500/42d	DTA, 500°C
	B6.5	$Cu_{75}As_{12.5}Sb_{12.5}$	-	-	-	x	-	x	-	-	x	-	-	-
	B7	$Cu_{72}As_{14}Sb_{14}$	-	-	450, 550	x	x	x	-	-	x	x	450 & 550/30d	DTA, as-cast, 450°C, 550°C
	B7.5	$Cu_{70}As_{15}Sb_{15}$	-	-	-	x	-	x	-	-	x	-	-	DTA
	B8	$Cu_{68}As_{16}Sb_{16}$	-	-	-	x	x	x	-	-	x	-	-	DTA, as-cast
	B9	$Cu_{68}As_{17}Sb_{17}$	-	-	-	x	x	x	-	-	x	x	-	DTA, as-cast
Cu-C (C=$AsSb_3$)	C1	$Cu_{96}As_1Sb_3$	x	x	-	x	-	x	x	x	-	-	-	500°C
	C2	$Cu_{92}As_2Sb_6$	x	x	-	x	-	x	x	x	-	-	-	500°C
	C3	$Cu_{88}As_3Sb_9$	x	x	-	x	x	x	x	x	-	-	500/42d	DTA, 500°C
	C4	$Cu_{84}As_4Sb_{12}$	x	x	-	x	x	x	x	x	-	-	-	DTA, 500°C, as-cast
	C5	$Cu_{80}As_5Sb_{15}$	x	x	350	x	-	x	x	x	-	x	350/18d; 500/42d	500°C
	C6	$Cu_{76}As_6Sb_{18}$	x	x	350	x	x	x	x	x	-	x	350/18d; 500/42d	DTA, 500°C
	C7	$Cu_{72}As_7Sb_{21}$	-	-	-	x	x	x	-	-	x	x	-	DTA, as-cast
	C8	$Cu_{68}As_8Sb_{24}$	-	-	-	x	x	x	-	-	x	-	-	DTA, as-cast
	C9	$Cu_{64}As_9Sb_{27}$	-	-	-	x	x	x	-	-	x	x	-	DTA, as-cast
	S2:1	$Cu_{66.7}As_{11.1}Sb_{22.2}$	-	-	-	x	x	x	-	-	-	x	-	DTA, as-cast

Table 2. Overview on binary alloys prepared, their thermal treatments and analyses carried out (x), or in preparation (●).

Compound	Temp.	Time	Quenching	XRD	Rietveld	SEM	Metallography
Cu_3As	300°C	20 d	air	single crystal	biphasic (Cu_5As_2)	x	-
	350°C	13 d	air	single crystal; powder	single crystal	x	x
	400°C	4.5 d	air	powder	x	-	-
	400°C	14 d	no	powder	single phase	x	x
	500°C	16 d	air	powder	biphasic (Cu_5As_2)	x	x
	16d/500°C → 1d/750°C		water	powder	biphasic (Cu_5As_2)	●	●
	19 d 650°C		water	powder	x	●	●
	19d/650°C → 1d/750°C		air	powder	biphasic (Cu_5As_2)	-	-
	750°C	15 d	air	powder	●	x	x
	15d/750°C → 12d/300°C		air	powder	●	●	x
Cu_5As_2	350°C	7 d	water	powder	●	x	x
	680°C	8 d	water	powder	●	x	x
	7d/350°C → 12d/300°C		air	powder	-	●	x
	8d/680°C → 12d/300°C		air	powder	-	●	x
Cu_3Sb	660°C	7d	air	powder	-	x	x
Cu_2Sb	550°C	7d	air	powder	-	x	x

Table 3. Overview on further analyses carried out on selected binary and ternary samples (phase and crystallographic analyses and physical properties measurements).

analyses	Cu_3As	Cu_5As_2	$Cu_{9-x}(As,Sb)_3$ [C7]
DTA	750°C/15d	680°C/8d	
single crystal XRD	x		x
DSC	300°C/20d	680°C/8d	
electrical resistivity	300°C/20d		x
Seebeck effect	x		x
Magnetic susceptibility	300°C/20d; 400°C/4.5d; 500°C/16d		x

4.2 Sample characterisation

4.2.1 Microstructure analyses (LOM)

Metallographic samples were embedded in cold mounting acrylic resin (Struers, ClaroCit Kit), grinded with abrasive papers (up to 1200 mesh) and polished with diamond paste down to 1µm. Microstructure analyses were carried out with a light optical microscope (LOM; **Leica DM1750M**) with up to 1000x magnification both in bright field and polarized light.

4.2.2 Chemical analyses (SEM-EDXS)

The chemical composition of the alloys and single phases were evaluated with an SEM-EDXS at the CNR-SPIN at Genova. The SEM-EDX used was a **Thermionic Scanning Electron Microscope** (Leica Cambridge S360) with an EDS system consisting of a large area analytical Silicon Drift Detector (**Oxford X-Max20**). Analysis were performed with a SEM acceleration voltage of 20.0 kV and probe current 220 pA, using an acquisition time of 100 seconds. As standards, pure Co and Cu metals were used for calibration. The overall area of the specimen (15-20 mm^2) was used as standard of known composition to correct the accuracy of the measurements, which in this way was estimated to be within 0.5-1.0 at.% for each element. The used analytical software was AztecEnergy.

4.2.3 Differential Thermal Analyses (DTA)

Samples of 0.65 – 0.75 g were cut for DTA (model: **NETZSCH DTA 404 S**). The samples were placed in Al_2O_3 crucibles, and covered with an Al_2O_3 lid and an additional cap prepared of pure Cu (6N) foil, to capture small amounts of As-vapour that could be released especially from As-rich alloys (see **Table 4** in **section 5.1**). Each sample was heated under Ar up to about 100°C above its melting temperature (previous observation of the sample during synthesis already gave a good indication of the approximate melting temperature +/- 50°C) and usually held for 5 minutes. Cooling rates were fixed at 5 and 10 K/min, the first preferred for cooling. In order to better visualize the peaks, also 2 K/min were used in single cases. For the measured temperatures, the accuracy was estimated to be within be ±3 °C for T ≤ 700 °C, and ±5 °C T for > 700 °C. No contamination of the alloy by the crucible material was observed by SEM-EDXS. Exothermic reactions and transformations that occurred during the solidification

process were recorded and plotted. The data acquired during cooling provided the liquidus, solidus, eutectic and peritectic transformations and reactions for each run.

4.2.4 Differential Scanning Calorimetry (DSC)

Differential scanning calorimetry was carried out on both single crystalline and polycrystalline bulks (10-30 mg in Al crucibles) by using a **TA Instruments DSC250 Discovery** under a N_2 flux of 50 mL/min. Heating and cooling runs were performed at 5 or 10 °C/min spanning a temperature range from -80 to 40 °C for LT and, above room temperature, up to 400°C.

4.2.5 X-Ray powder diffraction (XRD)

Powders were prepared by grinding polycrystalline pieces and placing them on a single-crystal Si zero background sample holder. The samples were analysed using the following instruments:

- Most X-ray powder patterns (XRPD) were collected on a **Bruker D4 Endeavour** diffractometer (Cu Kα radiation) equipped with an area detector (generally within 2θ ranges of 5-100°, in step size of 0.02° and a counting time of 4 or 6 sec/step). Pure Si was used as an internal standard [a = 5.4308(1) Å].
- Additionally, some samples were analysed with a Panalytical **X'PERT PRO** diffractometer (at the CNR-SPIN, Genova) with Cu-Kα radiation (λ = 1.54056 Å), operating at 40 kV and 30 mA; a range from 5-110 degrees 2θ was scanned with a step size of 0.001° and a counting time of 30 s per step. Pure Si was used as internal standard [a = 5.4308 Å].

The patterns were indexed by the help of **Lazy Pulverix** software [45] and accurate lattice parameters calculated by means of least-square methods (handmade software). Rietveld structural refinements were carried out on selected patterns by using **FullProf** software [46].

4.2.6 Single crystal X-ray diffraction (XRD)

On selected samples, also single crystal XRD was carried out. Single crystals were selected under the optical microscope from crushed sample pieces and affixed to a glass fibre with grease. The composition of the same crystal was also checked by SEM-EDX. Single crystals were analysed using a **Bruker D8 Quest diffractometer with a Kappa APEXII detector**. The

crystals were tested at room temperature on the diffractometer, equipped with a CCD area detector and graphite monochromatized Mo-Kα (λ = 0.071073 Å) radiation (with Mo-Kα radiation; λ = 0.71073 Å). The intensity data were collected over the reciprocal space in between 2 and 45° of 2θ with exposures of 20 sec. per frame. Further measurements were carried out in low-temperature down to 150 K. For the visualisation of the atomic structure, the program **Diamond** was used.

4.2.7 Transport/physical property measurements

Electrical resistivity and Seebeck effect were measured in cooperation with F. Caglieris (DIFI, UNIGE) using the commercial apparatus Physical Properties Measurement System (**PPMS, Quantum Design**) with home-made sample holders (**Figure 6**).

The electrical resistivity has been measured in a standard four-probe configuration, experimentally realized with copper leads glued on the sample through silver paint, in a temperature range between 2 – 310 K and magnetic field up to 9 Tesla (*T*). In the Seebeck effect setup, one side of the sample has been anchored to a thermal mass, while a resistive heater (R=2.8 kOhm) has been glued on the other side in order to generate a temperature gradient. A calibrated Chromel-Au-Chromel thermocouple has been used to measure the temperature gradient across the sample, while two copper electrodes have been attached to the sample to pick up the Seebeck voltage. The Seebeck data have been collected in between 15 – 290 K.

Magnetic susceptibility was measured in cooperation with F. Caglieris (DIFI, UNIGE) both on a single crystal and on a polycrystalline sample of Cu_3As and $Cu_{9-x}(As,Sb)_3$, using the commercial apparatus **SQUID (MPMS, Quantum Design)**. The temperature-dependent magnetization measurements were acquired from 5 – 300 K and in external magnetic fields of 1 *T*. The samples analysed are the following:

- $Cu_{9-x}(As,Sb)_3$ (C7_DTA; $Cu_{72}As_7Sb_{21}$): electrical resistivity, Seebeck effect, magnetic susceptibility;
- Cu_3As: electrical resistivity, Seebeck effect, magnetic susceptibility.

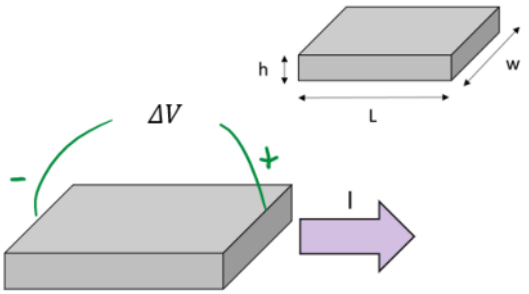

$$\rho = \left(\frac{\Delta V}{I}\right)\frac{hw}{L} \qquad RRR = \frac{\rho(300K)}{\rho(10K)}$$

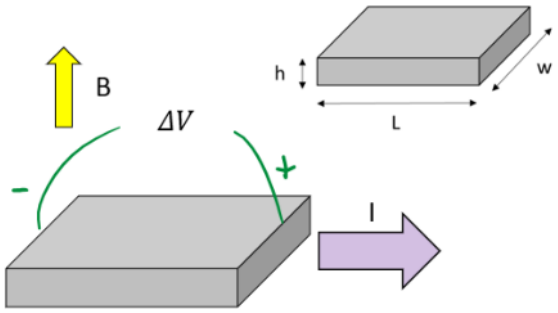

$$MR = \frac{\rho(B) - \rho(0)}{\rho(0)}$$

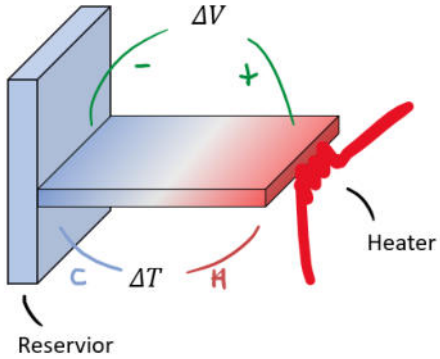

$$S = -\left(\frac{\Delta V}{\Delta T}\right)$$

Figure 6. Principle of the transport/physical property measurements carried out. **top**: resistivity measurements. **Centre**: magnetoresistance. **bottom**: Seebeck.

5. Results and discussion

5.1 Microstructure and chemical analyses (LOM and SEM-EDXS)

The chemical composition of the different parental alloys was determined by SEM-EDXS analyses on various metallographic specimens, preferably the ones which underwent thermal treatment, and/or DTA samples, as this eased the correlation with the DTA data and LOM evaluation of different phases. **Table 4** indicates the results of all EDXS data, which almost all match well the nominal composition (see below), especially when taken into account detection limits and accuracy of the instrument used.

Table 4. Overview on SEM-EDXS analyses carried out on the global composition of the 31 parental alloys as-cast and after different thermal treatments (values rounded at the first decimal).

name	alloy	nominal			as-cast			DTA			300°C (A) 350°C (B, C)			450°C			500°C			550°C		
		Cu	As	Sb	Cu	As	Sb	Cu	As	Sb	Cu	As	Sb	Cu	As	Sb	Cu	As	Sb	Cu	As	Sb
A1	$Cu_{96}As_3Sb_1$	96	3	1													96.4	2.6	1.0			
A2	$Cu_{92}As_6Sb_2$	92	6	2													91.8	5.9	2.3			
A3	$Cu_{88}As_9Sb_3$	88	9	3													87.5	9.2	3.3			
A4	$Cu_{84}As_{12}Sb_4$	84	12	4				84.0	11.7	4.3							83.5	12.1	4.4			
A5	$Cu_{80}As_{15}Sb_5$	80	15	5				80.1	14.6	5.3	81.0	14.1	4.9				79.3	15.3	5.4			
A6	$Cu_{76}As_{18}Sb_6$	76	18	6				75.9	17.7	6.4	77.7	16.5	5.8				75.4	18.1	6.6			
A7	$Cu_{72}As_{21}Sb_7$	72	21	7	71.7	21.0	7.3	72.6	20.2	7.2				74.4	18.8	6.7				74.5	18.7	6.8
A8	$Cu_{68}As_{24}Sb_8$	68	24	8	68.0	23.5	8.5	67.9	23.3	8.8												
A9	$Cu_{64}As_{27}Sb9$	64	27	9	64	25.8	10.2	62.9	25.6	11.6												
B1	$Cu_{96}As_2Sb_2$	96	2	2													96.0	2.0	2.0			
B2	$Cu_{92}As_4Sb_4$	92	4	4													91.3	4.4	4.3			
B3	$Cu_{88}As_6Sb_6$	88	6	6													87.8	5.9	6.3			
B4	$Cu_{84}As_8Sb_8$	84	8	8	85.6	5.8	8.6										86.2	**5.2**	8.6			
B4.5	$Cu_{82}As_9Sb_9$	82	9	9																		
B5	$Cu_{80}As_{10}Sb_{10}$	80	10	10							81.1	9.1	9.8				80.5	9.3	10.2			
B6	$Cu_{76}As_{12}Sb_{12}$	76	12	12				75.8	11.7	12.5	77.6	10.7	11.7				74.4	12.5	13.1			
B6.5	$Cu_{75}As_{12.5}Sb_{12.5}$	75	12.5	12.5																		
B7	$Cu_{72}As_{14}Sb_{14}$	72	14	14	71.7	13.9	14.4	71.2	14.0	14.8				74.1	12.5	13.4				73.5	13.0	13.5
B7.5	$Cu_{70}As_{15}Sb_{15}$	70	15	15				68.9	14.8	16.3												
B8	$Cu_{68}As_{16}Sb_{16}$	68	16	16	67.1	15.3	17.6	68.2	15.0	16.8												
B9	$Cu_{64}As_{18}Sb_{18}$	64	18	18	61.7	17.4	21	62.5	16.7	20.8												
C1	$Cu_{96}As_1Sb_3$	96	1	3													95.8	1.1	3.1			
C2	$Cu_{92}As_2Sb_6$	92	2	6													91.4	2.1	6.5			
C3	$Cu_{88}As_3Sb_9$	88	3	9				87.7	2.9	9.4							87.3	3.0	9.7			
C4	$Cu_{84}As_4Sb_{12}$	84	4	12	82.7	4.1	13.2	82.7	4.1	13.2							83.4	3.5	13.1			
C5	$Cu_{80}As_5Sb_{15}$	80	5	15							80.8	4.6	14.6				79.3	4.8	15.9			
C6	$Cu_{76}As_6Sb_{18}$	76	6	18				76.0	5.9	18.1	76.6	6.0	17.4				75.7	6.0	18.3			
C7	$Cu_{72}As_7Sb_{21}$	72	7	21	71.5	6.7	21.8	71.3	7.2	21.5												
C8	$Cu_{68}As_8Sb_{24}$	68	8	24	67.0	8.1	24.9	67.6	7.9	24.5												
C9	$Cu_{64}As_9Sb_{27}$	64	9	27	62.6	8.9	28.5	62	9.7	28.3												
S2:1	$Cu_{66.7}As_{11.1}Sb_{22.2}$	66.7	11.1	22.2	65.8	11.0	23.2															

Of interest is a slight change in the chemical composition especially of samples rich in As (Group A); a loss of As during synthesis is notable, as during the annealing at 500°C/month (see for instances samples A4-A6; B4;). The loss of arsenic during DTA analyses was moreover proven by the formation of Cu_3As-crystals on the inside of the Cu-cap, which covered the lid of the Al_3O_2-crucible in order to avoid the presence of As in the DTA-chamber (amongst others, namely samples A9 and B9).

Combining SEM-EDXS analyses with the microstructural images obtained by LOM, several different phases could be identified; these are indicated in **Figures 7 to 13** and **Table 5**. It is worth noting that not all over 200 metallographic samples underwent analyses via SEM-EDXS but only a selected number, i. e. about 75 specimen.

The **identified phases of the Cu-As-Sb system** (**Table 5**) go well beyond the actual planned study limits of 64-100 at.% Cu, as also as-cast samples far from equilibrium were studied. In **Figures 8** and **9** an overview of all so far through SEM-EDXS detected phases and eutectics is presented. **Figure 9** focusses on the copper-rich corner of the Cu-As-Sb system (64-100 at.% Cu), as was the study aim of the thesis. In this area, we note four main phases: Cu(α), Cu(AsSb), the hexagonal phase *hP*24, a cubic phase *cP32* and a tetragonal phase *tP*6. Their solubility for both As and Sb is rather wide, resulting in subgroups A-C for *hP*24 and *cP32*): Group A with As>Sb; Group B with As~Sb; and Group C with As<Sb. Four subgroups were defined for tP6. The unstable compound with the approximate composition $Cu_{11}(As,Sb)_3$, likely forming at circa 600°C and decomposing peritectoidally at circa 400°C, still awaits confirmation through XRD-analyses.

Looking at the Sb-rich alloys synthesized, intermetallic compounds and eutectics of the Sb-rich corner of the Cu-As-Sb system were discovered and their chemical composition documented. At least three eutectics (D, E and F) were identified, as well as three different Sb-rich phases with the approximate composition of As_3Sb_7, $Cu_{18}As_9Sb_{73}$ and $Cu_{14}As_6Sb_{80}$, and Sb(α) were documented and are currently in preparation as parental alloys for further analyses. The investigation and the study of this area of the Cu-As-Sb system, as well as the As-rich corner of it, will be in the focus of the just started MSCA-fellowship of M. Mödlinger.

The chemical composition of further single phases forming eventually other eutectics were identified; the global composition of these eutectics will be further investigated and confirmed through DTA and SEM-EDXS analyses during the MSCA-fellowship of M. Mödlinger.

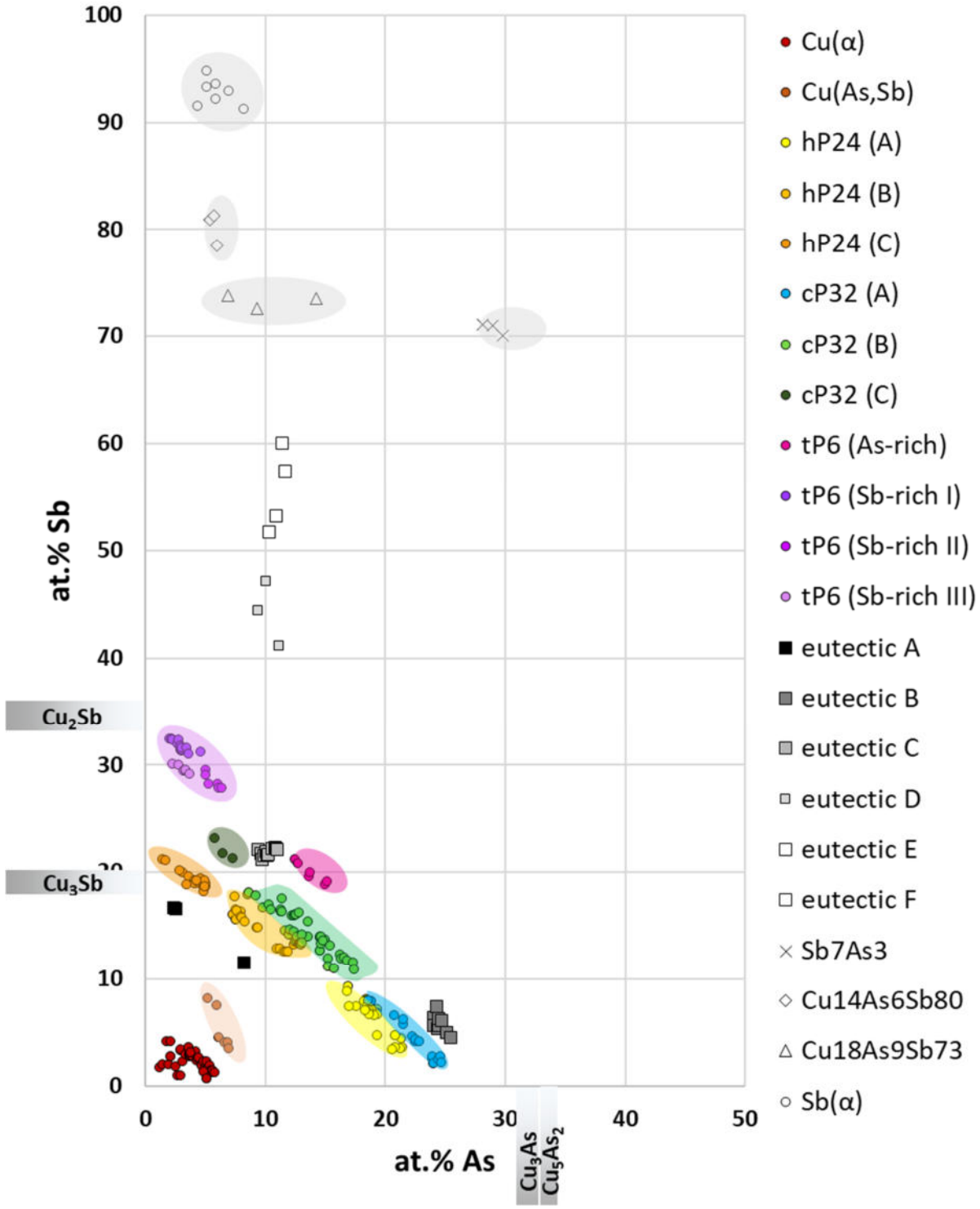

Figure 7. Phases detected according to their chemical composition (SEM-EDXS analyses).

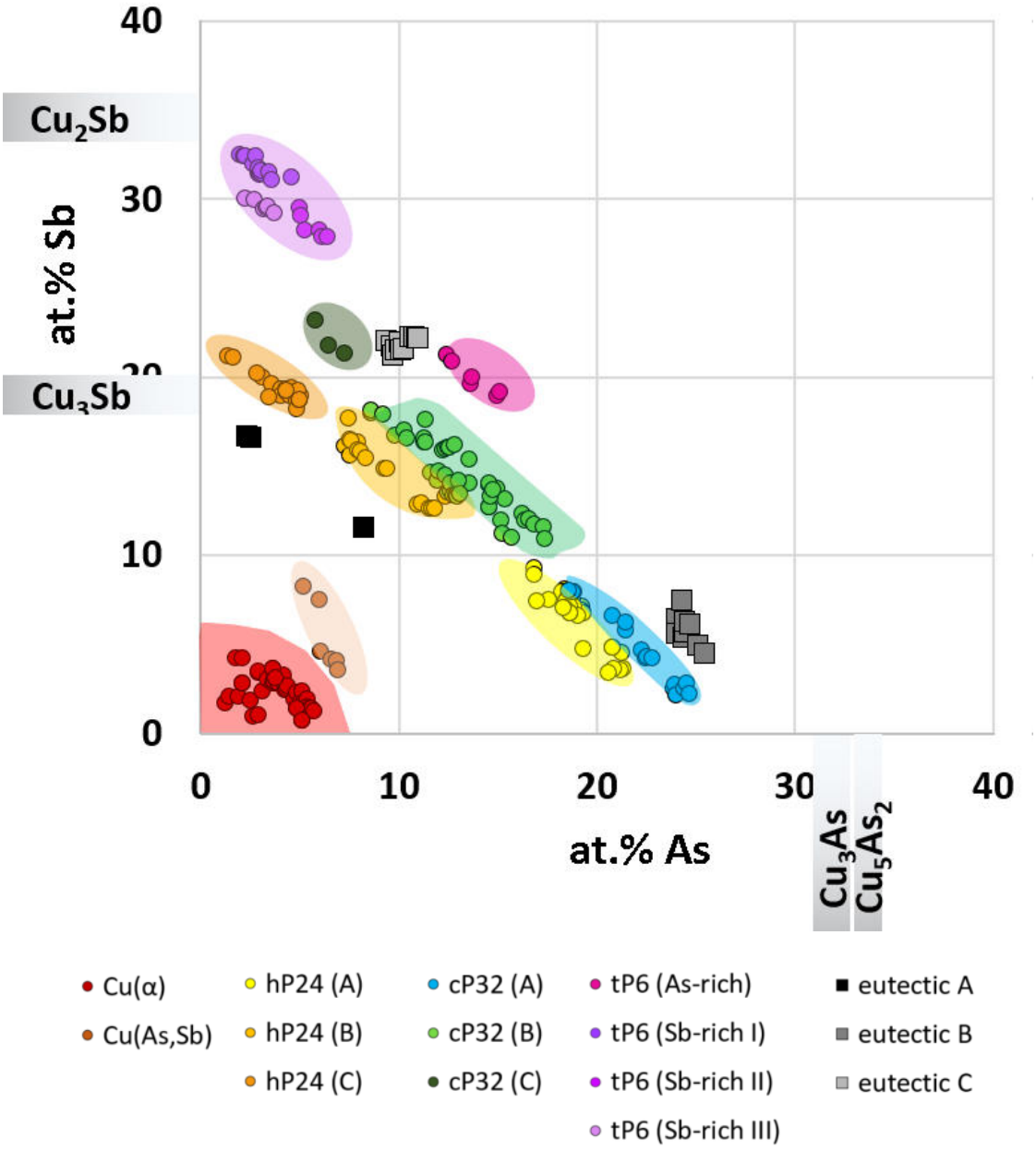

Figure 8. Phases detected according to their chemical composition (SEM-EDXS analyses). Detail of **Figure 7**.

Table 5. Phases of the Cu-As-Sb system as detected via LOM and SEM-EDXS.

phase	phase details	Cu at.%	As at.%	Sb at.%	analyses	present in sample
Cu(α)	**Cu(α)**	92.6 – 97.1	1.3 – 5.8	0.6 – 4.2	47	**as-cast**: A4, B4, C4; **300°C**: A5-6; **350°C**: B5; **500°C**: A1-2, A4-6, B1-6, C2-5; **DTA:** A4-6, B4, B6, C3
Cu(AsSb)	**Cu(AsSb)**	86.5 – 89.6	5.2 – 6.9	4 – 8.2	6	**350°C**: B5, C5;**DTA**: A6, B6, C6
3 : 1 [$Cu_{3-x}P$] *hP*24	**A**	73.6 – 76	16.9 – 21.4	3.4 – 9.3	30	**as-cast**: A4; **300°C**: A5-6; **450°C**: A7; **500°C**: A2-6; **550°C**: A7; **DTA**: A4-6, B9
	B	74.8 – 76.9	7.5 – 11.9	12.6 – 17.7	17	**as-cast**: B4; **350°C:** C5; **500°C**: B3-6, C5-6
	C	75.9 – 77.6	1.4 – 5.1	18.2 – 21.2	22	**as-cast**: C4; **500°C**: B3-6, C2-6; **DTA**: C3, C4, C6
circa 5 : 2 [Cu_9TeSb_2] *cP32*	**A**	72.3 – 73.5	20.8 – 24.5	2.1 – 6.6	16	**as-cast**: A7-9; **DTA**: A7-9
	B	71.1 – 73.5	8.6 – 17.4	10.9 – 18.1	49	**as-cast:** A4, A7, B7, B8, C8, C9, S2:1; **350°C**: B5-6; **450°C**: B7; **500°C**: B3-6; **550°C**: B7; **DTA**: A4, A6-7, B6-7, B7.5, B8, C6, S2:1
	C	71.1 – 71.8	5.8 – 7.3	21.3 – 23.1	3	**as-cast**: C7; **DTA**: C7
2 : 1 [Cu_2Sb] *tP*6	**pink**	65.8 – 66.8	12.5 – 15.1	18.9 – 21.2	7	**as-cast**: B7, S2:1; DTA:B7
	violet I	64.1 – 65.7	2 – 4.6	31 – 32.4	13	**as-cast**: C8, S2:1; **DTA**: B7.5, B8, C8, S2:1
	violet II	65.5 – 66.5	5.1 – 6.4	27.8 – 29.5	6	**as-cast**: A7, C7
	violet III	67 – 67.7	2.3 – 3.7	29.2 – 30	6	**as-cast**: C9; **DTA**: C9
Sb(α) *hR*6	**Sb(α)**	0 – 1.5	4.4 – 8.2	91.3 – 94.8	7	**as-cast**: C9, S2:1; **DTA**: B8, B9, C9, S2:1
As_3Sb_7	**As_3Sb_7 (3 : 7)**	0 – 1	28 – 29.8	70 – 71	3	**as-cast**: A9; **DTA**: A9
$Cu_{14}As_6Sb_{80}$	**$Cu_{14}As_6Sb_{80}$ (1 : 4)**	18.1 – 19.3	6.9 – 14.2	72.6 – 73-8	3	**DTA**: B7.5, A8
$Cu_{18}As_9Sb_{73}$	**$Cu_{18}As_9Sb_{73}$ (1 : 3)**	13 – 15.5	5.4 – 6.0	78.5 – 80.9	3	**DTA**: B7.5
eutectics	**A: Cu(α) + *cP32***	80.2 – 80.9	2.4 – 8.2	11.5 – 16.7	3	**350°C**: B6, C5
	B: ?	68.3 – 70.4	24 – 25.5	4.5 – 7.4	10	**as-cast**: A7-8; **DTA**: A8
	C: *tP*6 + *hR*6	67.2 – 69.1	9.4 – 11	21.2 – 24	11	**as-cast**: S2:1; **DTA**: C8, S2:1
	D: *tP*6 + Sb(α)	42.8 – 47.7	9.4 – 11.2	41.1 – 47.1	3	**as-cast**: B9; **DTA**: C9
	E: ?	35.9 – 37.9	10.4 – 10.9	51.7 – 53.2	2	**as-cast**: S2:1
	F: *tP*6 / *hP*24 (?) + Sb(α)	28.5 – 31	11.4 – 11.6	57.4 – 60	2	**as-cast**: A7, C8

In the following, **Figures 9 to 13** show selected images from the microstructural analyses via LOM and SEM-EDXS of the different phases detected in the copper-rich corner of the Cu-As-Sb system. Every figure is dedicated to one specific phase.

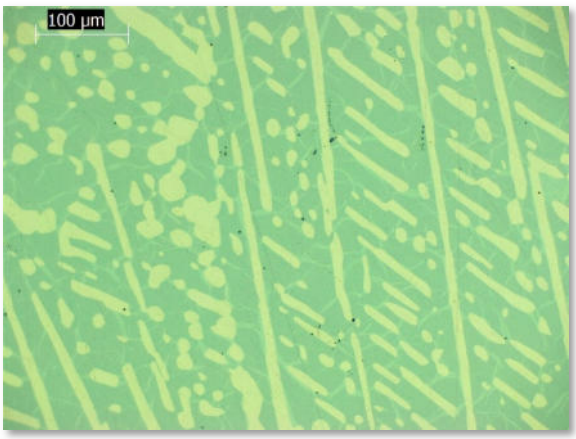

$Cu_{80}As_{10}Sb_{10}$ [B5], annealed a 500°C. Phases present: Cu(α) (yellow); *hP*24 (light green); ***cP32*** (dark green).

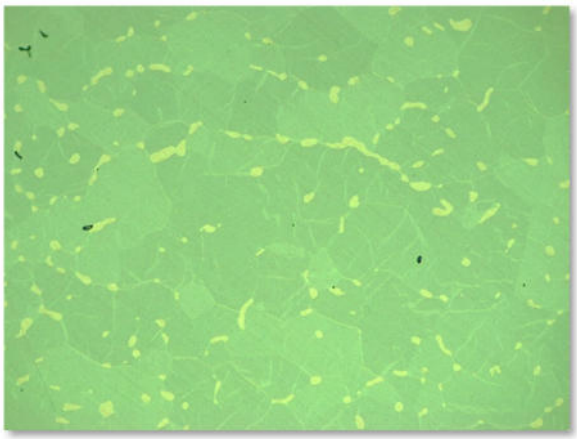

$Cu_{76}As_{12}Sb_{12}$ [B6], annealed a 500°C. Phases present: Cu(α) (yellow); *hP*24 (light green); ***cP32*** (dark green).

Figure 9. LOM- and SEM-EDXS images of the cubic phase $Cu_{9-x}(AsSb)_3$ [Cu_9TeSb_2], ***cP32***, space group *PM*3*m,* no. 223.

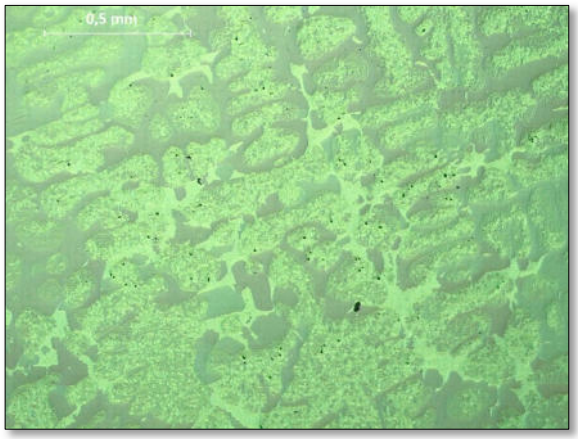

$Cu_{64}As_9Sb_{27}$ [C9], as-cast. Phases present: *tP*6 (pink and violet), eutectic (*cP32* (green) + ***hR6*** (white)); eutectic (*tP*6 and *cP32* (green)).

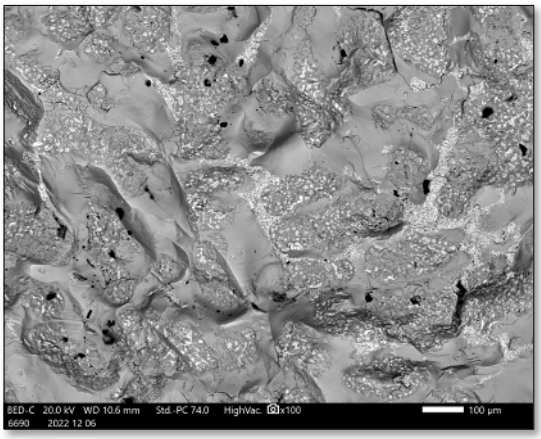

$Cu_{64}As_9Sb_{27}$ [C9], as-cast, not polished; SEM-EDXS image. Phases present: *tP*6 (grey), eutectic (*cP32* (dark grey) + ***hR6*** (white)); eutectic (*tP*6 and *cP32*).

Figure 10. LOM- and SEM-EDXS images of the rhombohedral phase Sb(As) [As] hR6, space group R-3m, no. 166

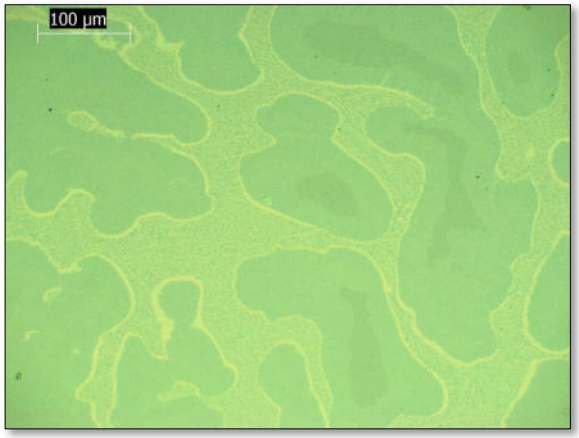

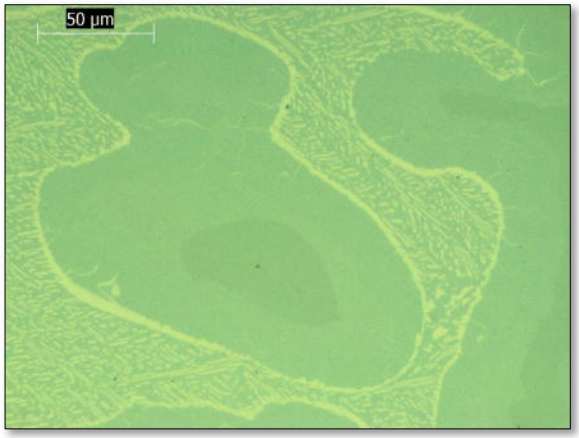

$Cu_{76}As_{12}Sb_{18}$ [B6], DTA. Phases present: ***hP*24** (various shades of green; the slight color differences are due to the different amounts of As present); Cu(α) (yellow) and eutectic (Cu(α) + ***hP*24**).

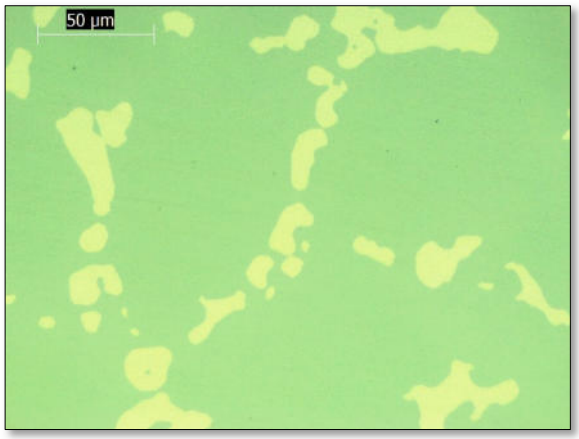

$Cu_{76}As_{18}Sb_{6}$ [A6], DTA. Phases present: ***hP*24** (green); Cu(α) (yellow).

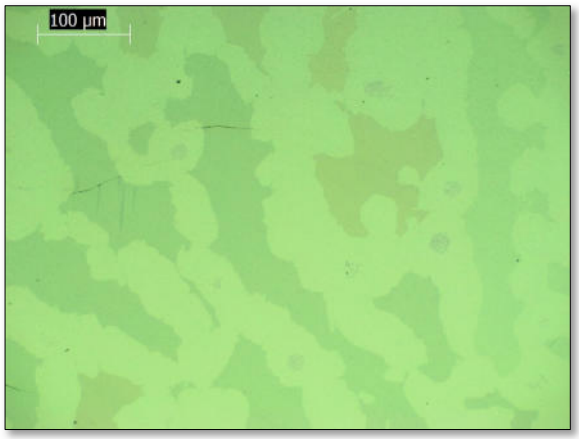

$Cu_{74}As_{21}Sb_{7}$ [A7], DTA. Phases present: ***hP*24** (various shades of green); eutectic (***hP*24** + *tP*6).

Figure 11. LOM images of the hexagonal phase $Cu_{3-x}(AsSb)$ [$Cu_{3-x}P$], ***hP*24** space group *P*63*cm*, no. 185.

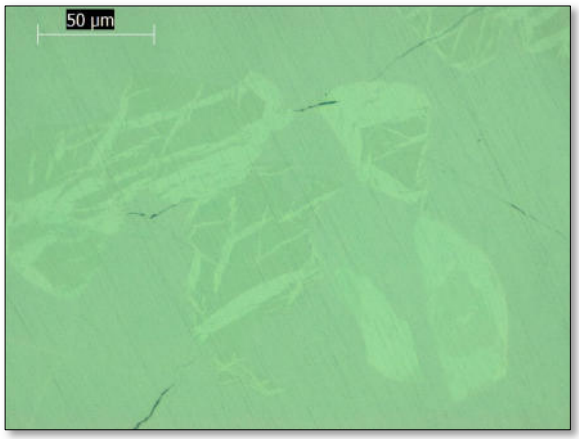

$Cu_{76}As_{6}Sb_{18}$ [C6], annealed a 500°C. Phase not yet fully identified; compound: $Cu_{11}(As,Sb)_3$.

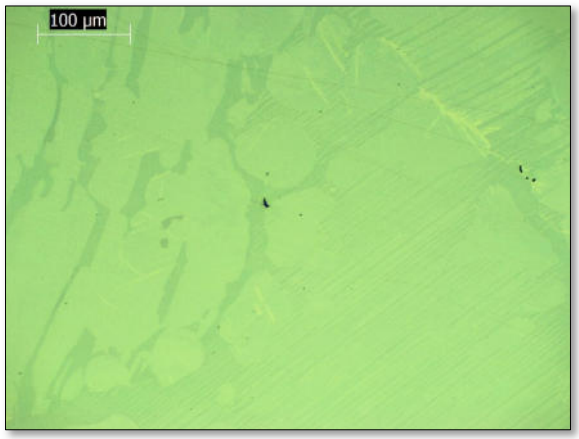

$Cu_{76}As_{6}Sb_{18}$ [C6], DTA. Phase not yet fully identified; compound: $Cu_{11}(As,Sb)_3$.

Figure 12. LOM- and SEM-EDXS images of the likely of the orthorhombic phase $Cu_{11}(As,Sb)_3$ [$Cu_{11}Sb_3$ – type, oI28, *Amm*2].

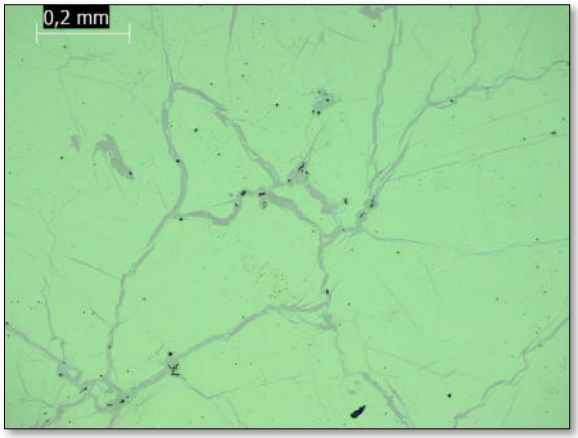

$Cu_{72}As_7Sb_{21}$ [C7], as-cast. Phases present: *cP32* (green); ***tP6***: pink (rich in As) and three different shades of violet.

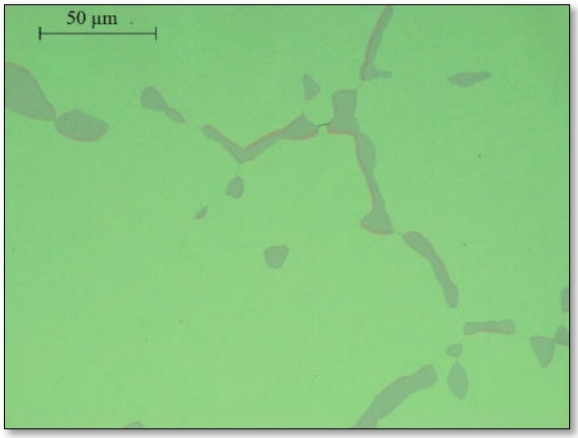

$Cu_{72}As_{14}Sb_{14}$ [B7], annealed at 450°C. Phases present: *cP32* (green); ***tP6***: pink (rich in As) and violet.

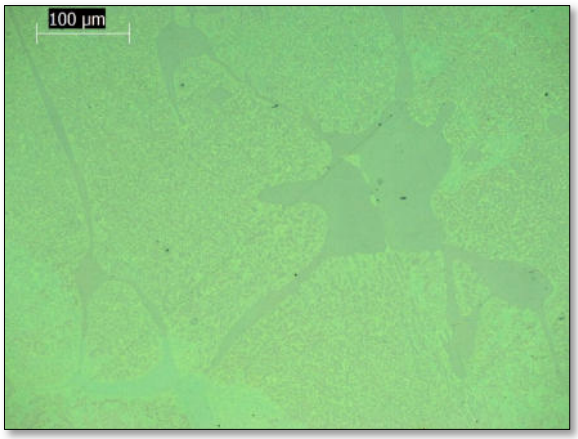

$Cu_{68}As_8Sb_{24}$ [C8], DTA. Phases present: ***tP6*** (pink and violet). eutectic (*cP32* (green) + ***tP6***).

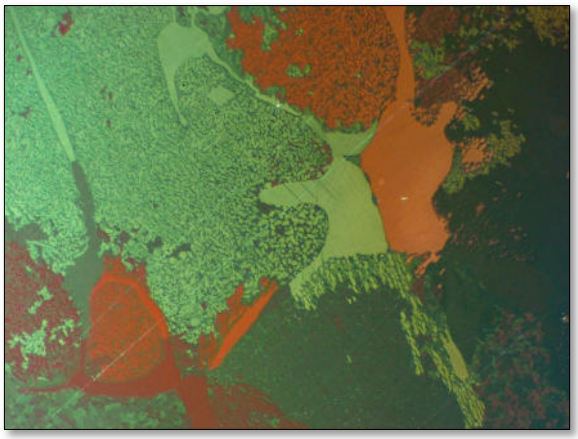

$Cu_{68}As_8Sb_{24}$ [C8], DTA; polarized light. Phases present: ***tP6*** (pink and violet). eutectic (*cP32* (green) + ***tP6***).

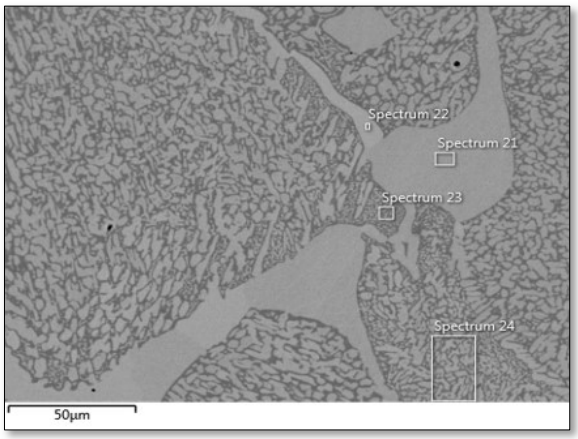

$Cu_{68}As_8Sb_{24}$ [C8], DTA, image SEM-EDXS. Phases present: ***tP6*** (grey and light grey), eutectic (*cP32* (dark grey) and ***tP6***).

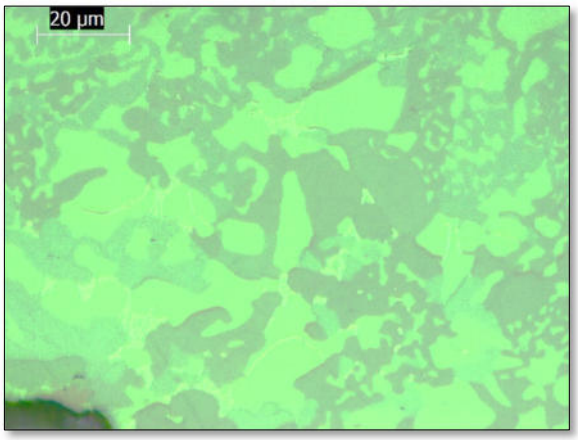

$Cu_{68}As_8Sb_{24}$ [C8], as-cast. Phases present: ***tP6*** (pink and violet I-III), eutectic (*cP32* (green) and ***tP6***).

Figure 13. LOM- and SEM-EDXS images of the tetragonal phase Cu_2(AsSb [Cu_2Sb], ***tP6*** space group *P4/nmm,* no. 129.

5.2 Differential Thermal Analyses (DTA)

The complete interpretation of data for the determination of the whole Cu-As-Sb system (pseudo-binaries and isothermal sections of the ternary system at 500°C) is still ongoing and needs the final confirmation from XRD, microstructural and SEM-EDXS data from the Sb- and As-rich corners of the Cu-As-Sb system, which were originally not part of the PhD-research. This part of the research will be continued during the MSCA-fellowship of M. Mödlinger.

In order to achieve further information about the stability of the different phases, and also to prepare samples closer to equilibrium conditions, i.e. with less different phases present, almost all samples underwent different annealing cycles, namely:

- 600°C: samples A1-6, B1-6 and C1-6. Annealing took place before DTA was carried out; this explains also the seemingly illogical annealing at 600°C, because the first eutectic of Group B and C takes place exactly at 600°C.
- 550°C: samples A7, B7
- 500°C: samples A1-6, B1-6 and C1-6
- 450°C: samples A7, B7
- 350°C: samples B5-6, C5-6
- 300°C: samples A5-6

These samples helped the evaluation and interpretation of the DTA data. Furthermore, they eased the comparison with data obtained from metallographic, SEM-EDXS and XRD data. DTA data points were extracted from the paper prints from the NETZSCH DTA 404 S (**Figure 14**).

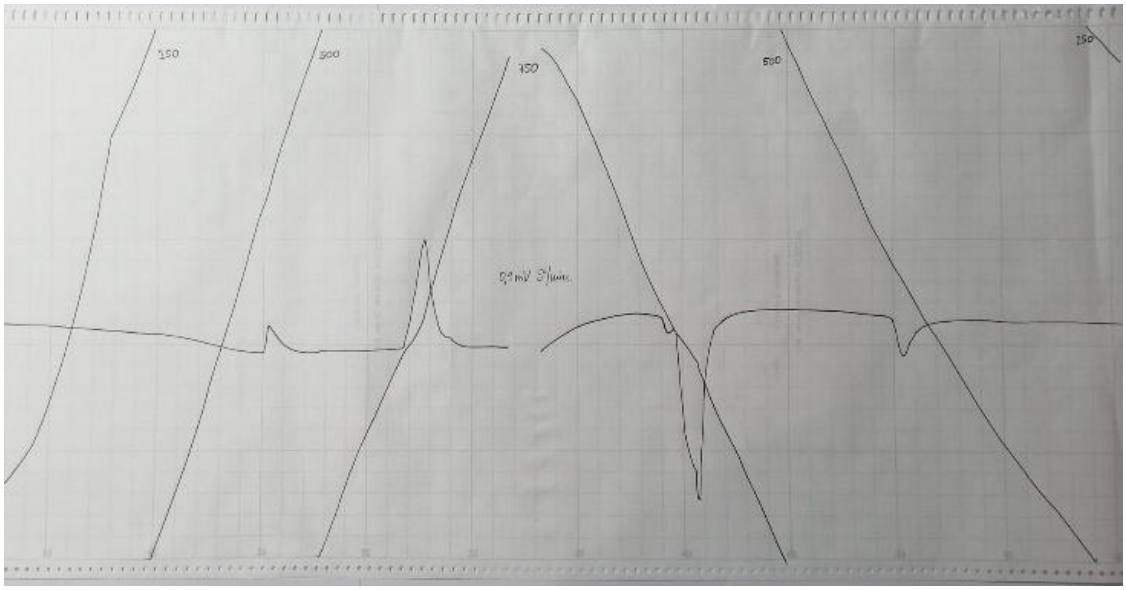

Figure 14. Example of one DTA-run used as a base for building the phase diagrams: sample C5. Reading starts at the left side of the image with the heating of the sample; at the centre of the image, cooling starts.

Figure 15 shows the provisional phase diagram of the Cu-As-Sb system, combined with the so far available data from XRD, metallographic and SEM-EDXS analyses.

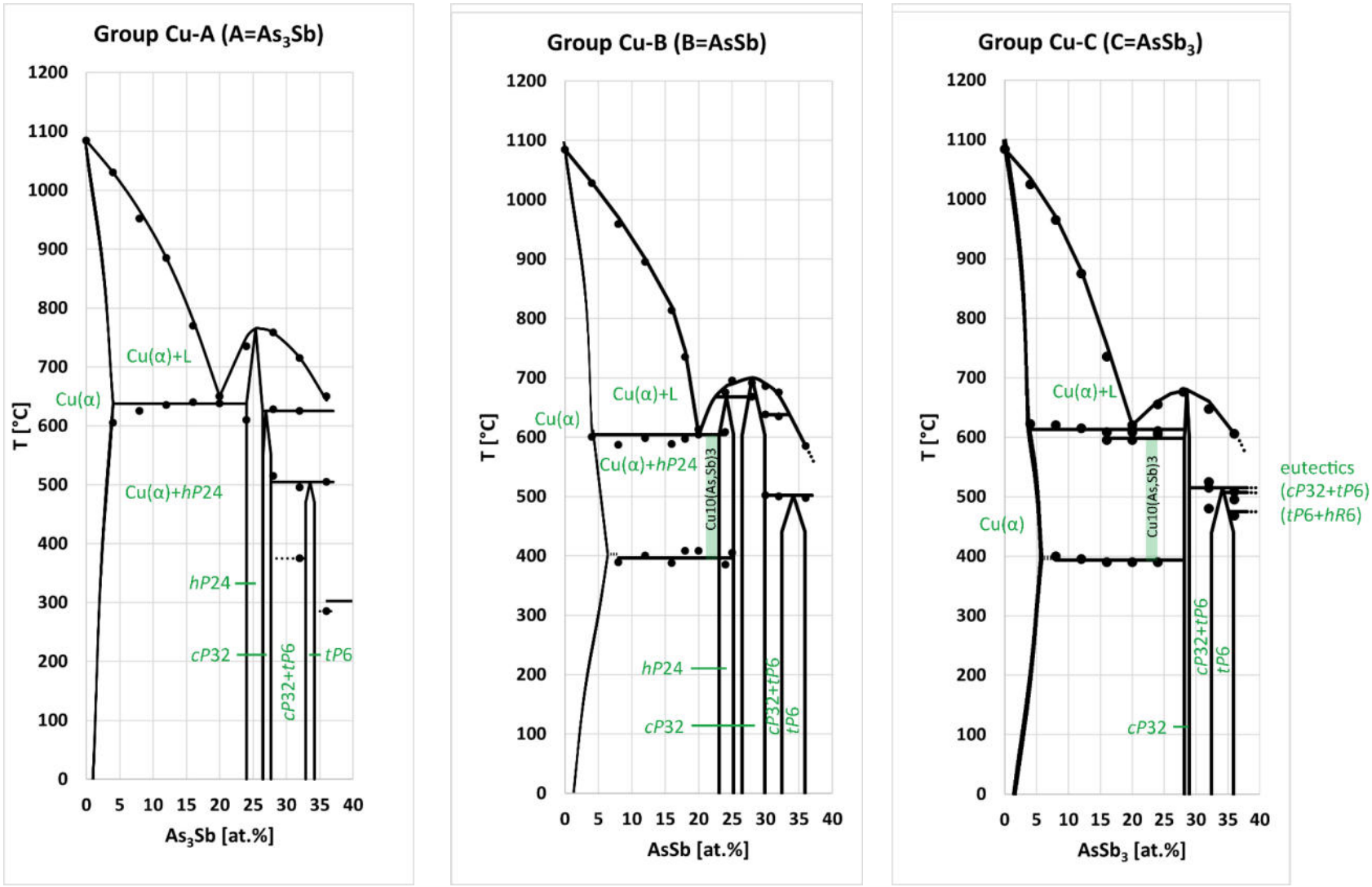

Figure 15. Provisional phase diagram of Group Cu-A, Cu-B and Cu-C pseudobinary systems. The lines do not yet fully represent equilibrium conditions; they only serve for a first rough visualization of trends. The compound $Cu_{10}(As,Sb)_3$ is not yet confirmed by XRD analyses.

5.3 Differential Scanning Calorimetry (DSC)

5.3.1 Cu_3As

Differential scanning calorimetry (DSC) was carried out on both single crystalline (annealed at 300°C for 20 days) and polycrystalline specimens of Cu_3As (**Figure 16**). A low-temperature phase transition is detected by a distinct thermal effect in differential scanning calorimetry, both in single crystals and bulk material. The associated enthalpy difference is of approximately 2 J/g. Very likely, this strongly relates to a change in the structure: the value of parameter *c* triples and probably parameter *a* doubles, as indicated by recent XRD analyses and a discontinuity of physical property measurements (**sections 5.4.2** and **5.5**). Final confirmation needs LT bulk heat capacity measurements and synchrotron diffraction (planned for 2023).

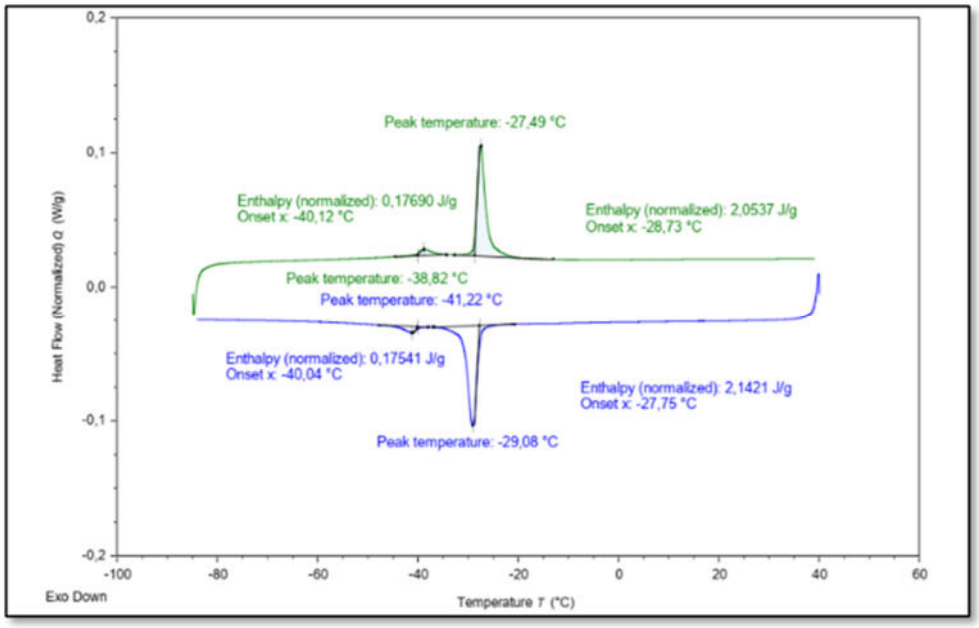

Figure 16. LT-DSC cooling (blue curve) and heating (green curve) runs at 5°C/min for a single crystal of Cu_3As (annealed at 300°C for 20 days). Endothermic heat flow direction is upward.

5.3.2 Cu_5As_2

Differential scanning calorimetry (DSC) was carried out with 5 and 10 K/min of a polycrystalline Cu_5As_2 sample (annealed at 680°C for 8 days) (**Figure 17**). The thermal effect detected at about 300°C is noted also from literature [22-23] and can be related either to the

decomposition of the compound or to a structural transition. Research continues to confirm or not confirm such literature data.

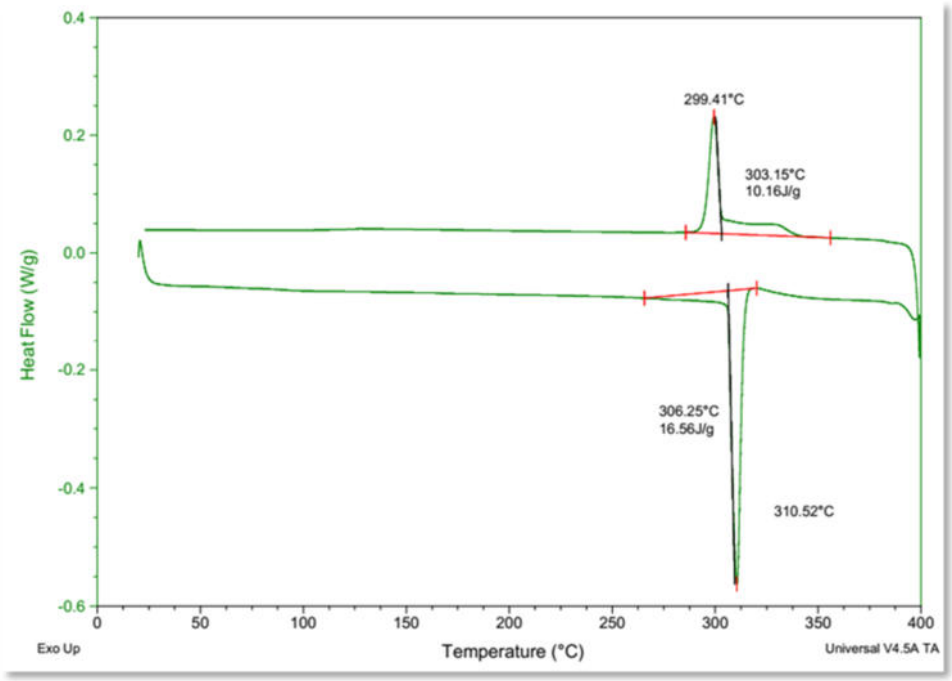

Figure 17. DSC heating runs at 5°C/min for a polycrystalline sample of Cu_5As_2 (annealed at 680°C for 8 days). Endothermic heat flow direction is downward.

5.4 X-ray powder and single crystal diffraction (XRD)

5.4.1 Cu-As-Sb system

Combining metallographic and SEM-EDXS analyses with XRD, several different phases and eutectics were detected in the Cu-As-Sb system. **Table 7** reports structure type, space group and Pearson notation, as well as lattice parameter and the unit cell volume of the different phases detected.

Note that all values of the lattice parameters of the *hP*24, *cP32* and *tP*6 compounds enlarge significantly with increasing amounts of Sb in the alloy (as Sb-atoms are significantly larger than As-atoms) (**Figure 18**).

Table 7. Lattice parameters and unit cell volume of the phases identified in the Cu-As-Sb system.

compound	sample	composition sample (at.%)	a Å	b Å	c Å	V_u Å^3
$Cu_{9-x}(AsSb)_3$ $[Cu_9TeSb_2]$ ***cP32*** Pm–3n. no. 223	A7_DTA II	$Cu_{72}As_{21}Sb_7$	7.465			416
	B7_as-cast	$Cu_{72}As_{14}Sb_{14}$	7.546			429.69
	B7_450°C	$Cu_{72}As_{14}Sb_{14}$	7.548			430.03
	B7_500°C	$Cu_{72}As_{14}Sb_{14}$	7.553			430.88
	C7_DTA single crystal	$Cu_{72}As_7Sb_{21}$	7.644			446.64
	C7_as-cast	$Cu_{72}As_7Sb_{21}$	7.652			448.05
$Cu_{3-x}(AsSb)$ $[Cu_{3-x}P]$ ***hP24*** $P6_3cm$, no. 185	A6_DTA	$Cu_{76}As_{18}Sb_6$	7.177		7.359	328.35
	B6_500°C	$Cu_{76}As_{12}Sb_{12}$	7.216		7.346	331.25
	A7_DTA_SH3	$Cu_{72}As_{21}Sb_7$	7.136		7.323	322.94
	B5_500°C	$Cu_{80}As_{10}Sb_{10}$	7.203		7.342	329.88
$Cu_2(AsSb)$ $[Cu_2Sb]$ ***tP6*** P4/nmm, no. 129	C8_DTA	$Cu_{68}As_8Sb_{24}$	3.982		6.077	96.36
	C9_DTA	$Cu_{64}As_9Sb_{27}$	3.99		6.091	96.96
	C7_DTA_1 run	$Cu_{72}As_7Sb_{21}$	3.992		6.097	97.14
Sb(As) [As] ***hR6*** R-3*m* no. 166	C9_DTA	$Cu_{64}As_9Sb_{27}$	4.282		11.219	178.14

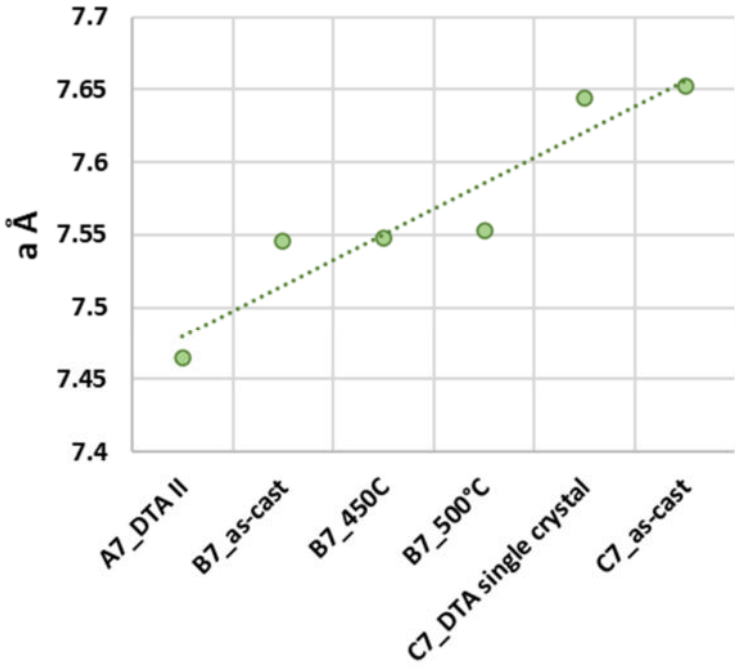

Figure 18. Trend of the lattice parameter *a* for the cubic $Cu_{9-x}(AsSb)_3$ compound.

Additionally to XRD analyses on powder samples, also Rietveld refinements were carried out on selected samples. Rietveld refinement on the most representative diffractograms were so far carried out on both the cubic and tetragonal main phases (*cP32* and *tP*6). Samples of alloys on the Sb-rich part of the ternary Cu-As-Sb system for further XRD and Rietveld analyses will be prepared during the MSCA-fellowship of M. Mödlinger in order to have a complete picture of all phases present in the Cu-As-Sb ternary system.

5.4.2.1 Phase $Cu_{9-x}(As,Sb)_3$: single crystal and powder analyses

A new ternary compound showing a very large solubility range with the composition $Cu_{9-x}(As,Sb)_3$ and crystallizing with the structure of $Cu_{9.1}(TeSb)_3$-type (*cP*32, *Pm*–3*n*, No. 223) was identified from single crystal analyses from the samples $Cu_{72}As_7Sb_{21}$ [C7_DTA] (**Figures 18 and 19**). The compound has a structure isotypic to that of $Cu_{9-x}TeSb_2$, a derivative of the Cr_3Si-type [47]. Standardized atomic coordinates and equivalent displacement parameters (Ueq) displacement parameters for $Cu_{9-x}(As,Sb)_3$ as obtained from powder pattern analysis from sample C7 from the new compound are reported in **Table 8**. The lattice parameter obtained from Rietveld refinement for $Cu_{9-x}(As,Sb)_3$ [a = 7.5146(1) Å] is smaller than that obtained from single crystal data [a = 7.644(2) Å], this indicating that more Sb atoms replaced As atoms in one or both the 6*c* and 2*a* Wyckoff sites (V_{Sb} = 29.97 Å^3 and, V_{As} = 21.52 Å^3). **Figure 19** shows the Laue pattern of the compound; the cubic structure is clearly visible.

Table 8. Standardized atomic coordinates and equivalent displacement parameters (U_{eq}) displacement parameters for $Cu_{3-x}(As,Sb)$ as obtained from single crystal analysis ($Cu_{72}As_7Sb_{21}$; sample C7_DTA). The isotropic displacement parameter, $U_{eq.}$, is defined as one third of the trace of the orthogonalized U_{ij} tensor.

Atom	Wyckoff site	*x*	*y*	*z*	Occ.	B_{iso} [Å^2]
Sb1	*6c*	1	1/2	1/4	0.859(2)	0.0189(2)
As1	*6c*	1	1/2	1/4	0.141(2)	0.0189(2)
Sb2	*2a*	1/4	1/2	1/2	0.32(2)	0.0253(6)
As2	*2a*	1/4	1/2	1/2	0.68(2)	0.0253(6)
Cu3	*24 k*	0.66385(13)	44593	0.20636(14)	0.8227	0.0269(3)

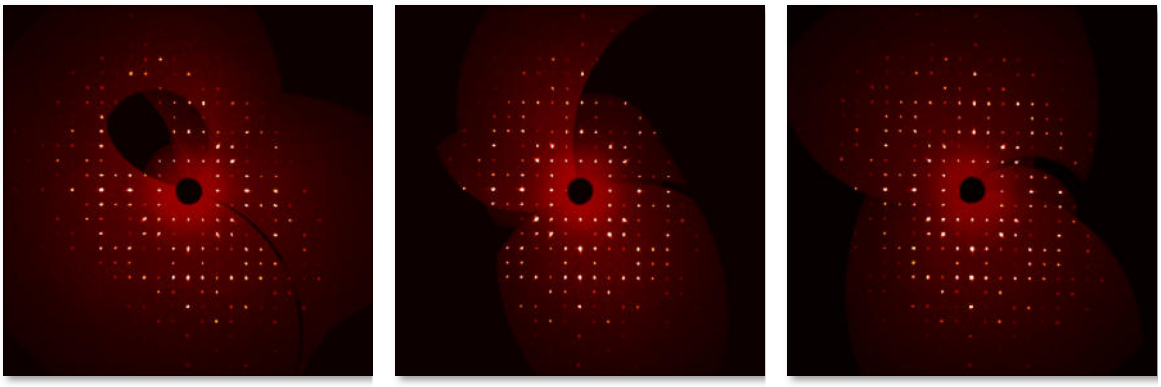

0kl **h0l** **hk0**

Figure 19. Laue patterns (reconstructed) of a single crystal of the cubic $Cu_{9-x}(As,Sb)_3$ compound [$Cu_{72}As_7Sb_{21}$; sample C7_DTA] . The cubic structure is clearly visible.

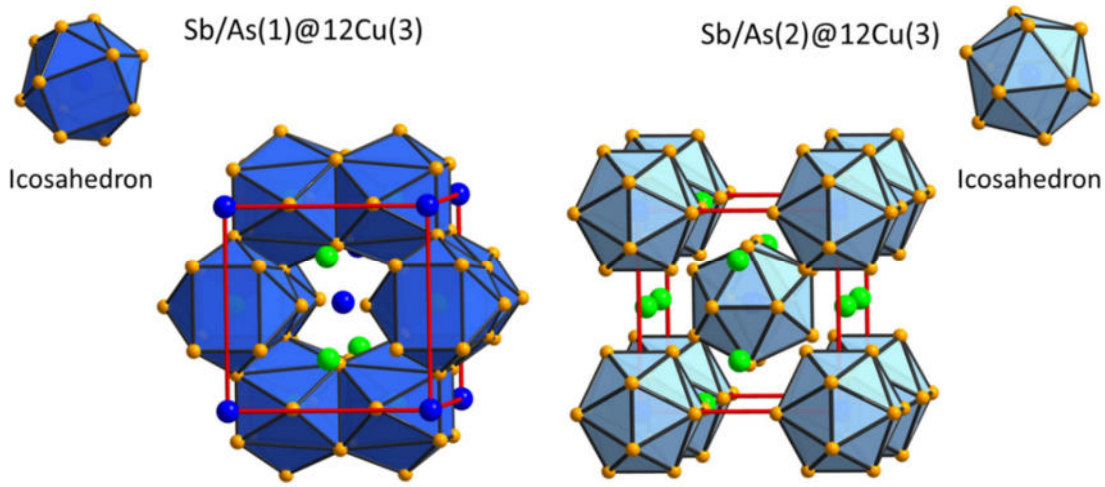

Figure 20. Perspective view of the crystal structure of the cubic compound $Cu_{9-x}(As,Sb)_3$. where the polyhedra around Sb/As(1) and Sb/As(2) (both Icosahedron) are highlighted.

The structure was confirmed by powder patterns from the samples $Cu_{72}As_{14}Sb_{14}$ [B7_550°C/42d] and $Cu_{72}As_7Sb_{21}$ [C7_DTA] refined through Rietveld methods (**Figure 21**).

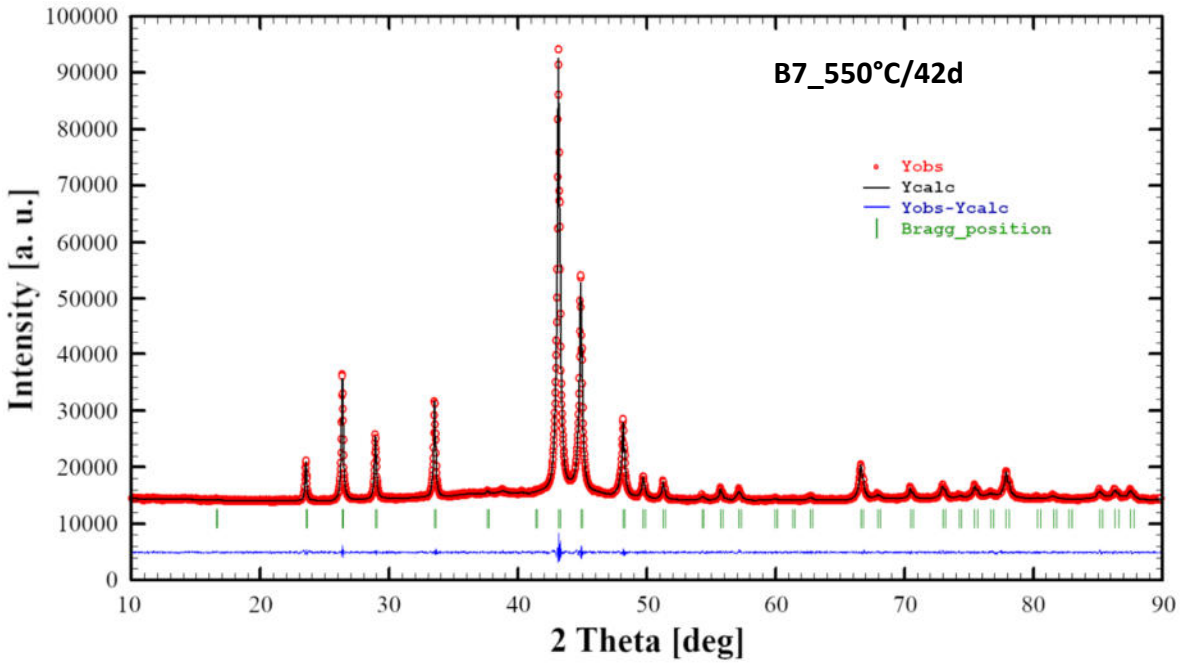

Figure 21. Observed X-ray powder pattern (red circle), and Rietveld refinement profile (black line) for the samples B7_550°C/42d. The lower profile (blue line) gives the difference between observed and calculated data; the Bragg angle positions are indicated by vertical bars (green). The sample is single phase containing the cubic $Cu_{9-x}(As,Sb)_3$ or compound [$Cu_{9.1}(TeSb)_3$-type, ***cP*32**, *Pm*–3*n*, No. 223].

5.4.2 Cu-As system: Cu_3As

As severe lacuna in the binary Cu-As system was detected, especially concerning the compounds Cu_3As and Cu_5As_2, analyses were carried out also on these intermetallic compounds. In effect, as discovered by XRD-analyses and Rietveld refinement, Cu_3As crystallizes in the hexagonal Cu_3P prototype (*hP*24, $P6_3cm$, No. 185), rather than in the anti HoH_3-type (or anti LaF_3-type) (*hP*24, *P*–3*c*, No. 165) as indicated in literature, with lattice parameters: a = 7.1393(1) Å and c = 7.3113(1) Å (powders). **(Figures 22** and **23**). Moreover, we also find that Cu_3As does not exist with other modifications at least up to 750°C (otherwise than what is so far reported in literature, see [22-23]).

Moreover, the data also revealed this compound to be slightly understoichiometric, with a final refined composition of $Cu_{2.882(1)}As$. The understoichiometry is associated with the vacancy in one of the four Cu positions only, and specifically one of the two 6*c* (**Table 10**).

X-ray diffraction on single crystal was also carried out at low temperature. The data showed a change in the crystal structure occurring at about 240 K. At 230-240 K, the data reveal an unit cell whose lattice parameter *a* is the same as per the Cu_3P-type, while parameter *c* is three times the value of the Cu_3P-type (with parameter *a* = 7.100(2) Å and parameter *c* = 21.870(5) Å).

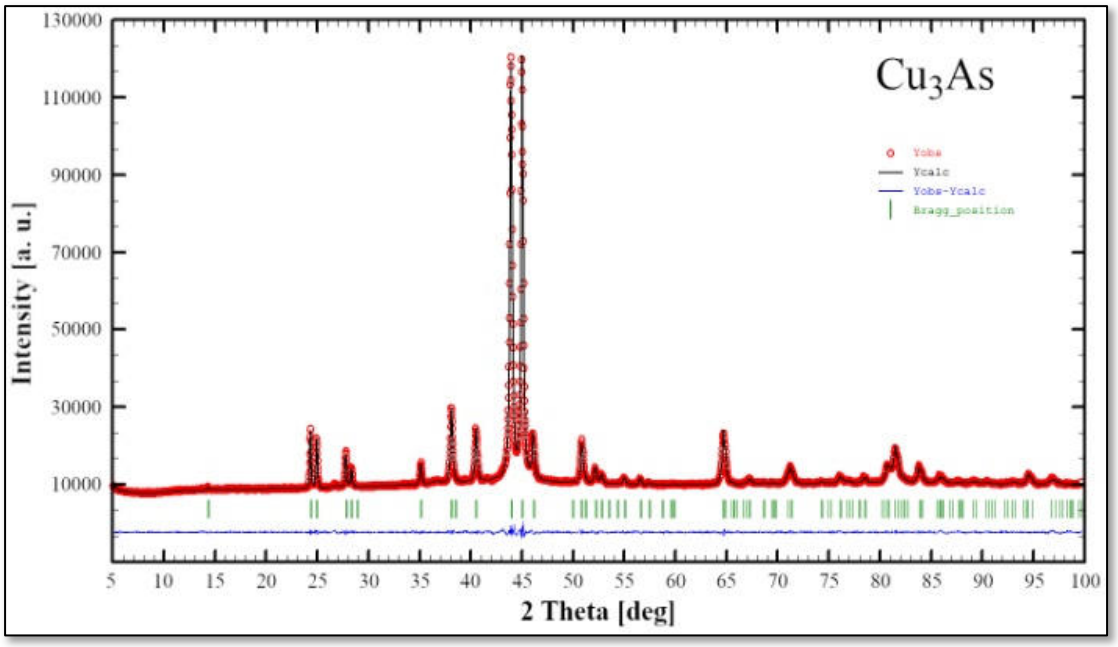

Figure 22. XRD-powder pattern (Rietveld refinement): Cu_3As (14 days at 400°C); hexagonal Cu_3P-type [*hP*24, $P6_3cm$ (No. 185)] at room temperature.

Table 10. Standardized atomic coordinates and equivalent displacement parameters (U_{eq}) displacement parameters for $Cu_{2.882(1)}As$ as obtained from single crystal analysis. The isotropic displacement parameter, $U_{eq.}$, is defined as one third of the trace of the orthogonalized U_{ij} tensor.

Atom	Site	Atomic coordinates			Occ.	U_{eq} [Å^2]
		x/a	*y/b*	*z/c*		
As	6*c*	0.33415(10)	0	0.0818(2)	1	0.01171(13)
Cu1	2*a*	0	0	–0.0004(4)	1	0.0209(3)
Cu2	4*b*	1/3	2/3	0.1546(4)	1	0.0376(5)
Cu3	6*c*	0.7121(2)	0	0.24994(13)	1	0.0237(2)
Cu4	6*c*	0.36808(19)	0	0.41244(15)	0.882(7)	0.0270(4)

Very interestingly, it can be observed that the room temperature structure of the Cu3As compound (RT-$Cu_{3-x}As$) is formed by two structural parts: (1) a 3D tridimensional network built up by the Cu2 and Cu3 atoms only; (2) slightly ondulated 2D layers of interconnected triangular 'Cu3As'-units, each unit formed by only Cu1 and Cu4 atoms at the three vertexes and hosting one As atom at the center.

The tridimensional network is made by the Cu2 (site 6c) and Cu3 (site 4b) atoms, which forms together an uncommon and peculiar sublattice of Cu atoms of the Lonsdaleite type. Lonsdaleite, also defined as hexagonal diamond (and, as well as, called meteor or impact diamond), is nowadays generally accepted by the scientific community as being one of the polymorph of carbon (aside hexagonal graphite and cubic diamond), despite its conditions of appearance and structural peculiarities still remain a bit controversial and questioned (because considered as cubic diamond dominated by extensive stacking faults and twins) [48]. Infact, at the present time, pure Lonsdaleite has never been found or synthesized as single crystal or in bulk form, but its presence, either from natural origin or artificial [synthesized in a laboratory under thermobaric (high dynamic/static pressure - high temperature, HP-HT) conditions [49], has been usually observed only in small amounts and as nanoparticles inside diamond crystals. Similarly to the structure of both cubic diamond and hexagonal lonsdaleite (where each *sp*3-hybridized carbon atom is bonded to four other carbon atoms), Cu2 and Cu3 atoms form a tetrahedral structure resulting in a 3D rigid network with stronger bonds. The four Cu2-Cu3 bond distances are: 2.531, 2.672, 2.672, 2.728 Å; values which are well comparable to the bond lengths in Cu metal [50] (see **Figure 23a**). Moreover, similarly to diamond and lonsdaleite, Cu atoms filling these two sites form puckered layers of atoms with six-members rings arranged in an armchair-like configuration (**Figure 23a**).

The triangular 'Cu3As'-units are formed by one Cu1 (2a) and two Cu4 (6c) atom placed at the 3 vertexes of an isosceles triangle (with angle values of about 57.6 deg and 61.2 deg, for respectively the the <Cu4-Cu1-Cu4> and <Cu4-Cu4-Cu1> angles). Each triangle hosts one As atom (in site 6c) centered onto the plane (with bond lengths of 2.460 Å and 2.436 Å, for the As-Cu1 and the two As-Cu4 bonds, respectively) and sets inside one three-rings cage of

the first tridimensional Cu sublattice (**Figure 24a-b**). Such triangles are interconnected three by three by sharing one Cu atom at the vertex, arranged slightly tilted each other but all facing to a same versus (**Figure 24c**), to finally form a structural layer (**Figure 24c-d**).

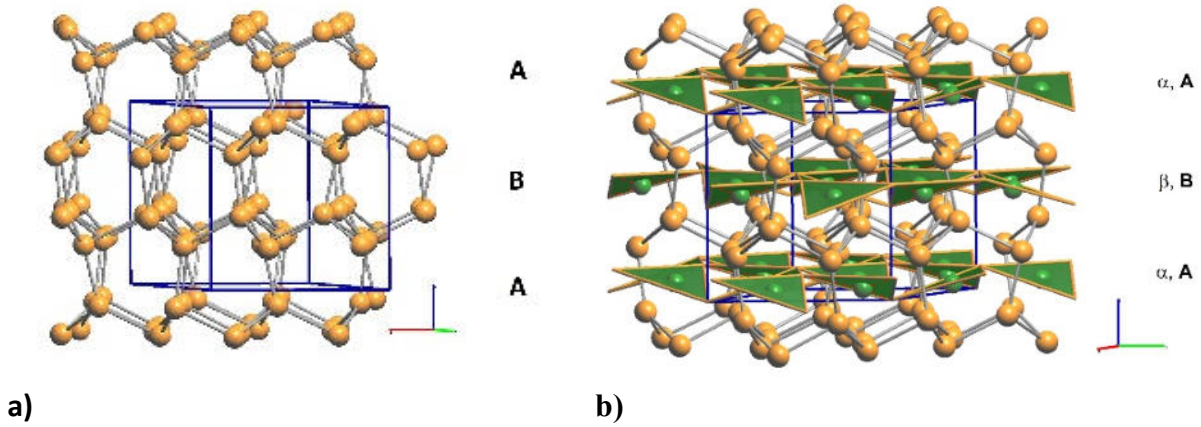

Figure 23. (a) Perspective view of the lonsdaleite type sublattice formed by the Cu2 and Cu3 atoms**. (b)** Perspective drawing of the RT-structure of the Cu_3As compound. Each unit cells contains two layers, α and β.

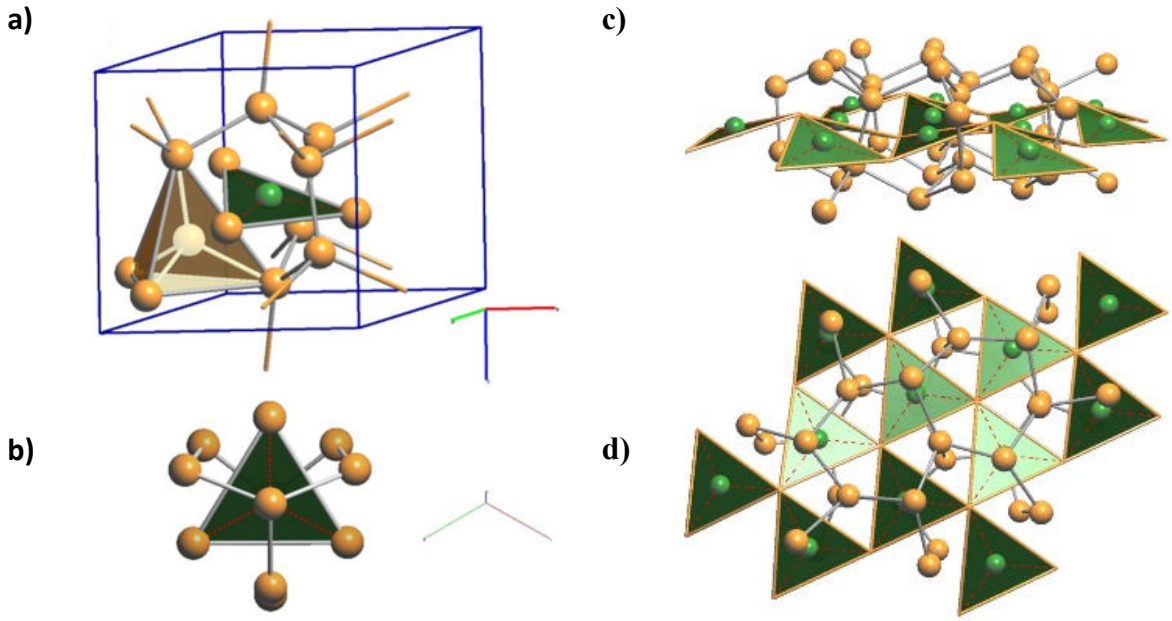

Figure 24. (a) Triangular 'Cu_3As'-units (Cu4-Cu1-Cu4), hosting one As atom (*6c*) and placed inside one three-rings cage of the first tridimensional Cu sublattice. **(b)** top view of one triangular unit. In **(a)** one tetrahedral unit formed by all Cu2 and Cu3 atoms, and pertaining to the lonsdaleite sublattice, is also shown. **(c)** perspective view of a layer formed by the Cu_3As-triangular units. **(d)** top view of the layer shown in (c).

The layers, in number of two by unit cell (α and β), are placed perpendicular to the c axis of the hexagonal cell, with the Cu atom interconnecting three 'Cu_3As' units centering the columnar cavities available along the c axis of the Cu sublattice (lonsdaleite-type network). Interlayer distance between layers α–β is 3.653 Å. The interatomic distances corresponding to the first coordination sphere (distances for which $d_{obs}/\Sigma r_M \leq 1.16$, where d_{obs} is the interatomic distance and Σr_M is the sum of the two metallic radii) are in Table 5; the structure does not present direct interactions As–As. Overall, the resulting crystal structure is shown in **Figure 23b**.

On the other hand, the structure of the RT-Cu3As phase could be also described as a complex array of pseudo Frank-Kasper polyhedra, with composition As@Cu11, connected with each other by sharing their triangular faces. **Figure 25** shows a sketch of the structure where these polyhedra around As atoms are highlighted.

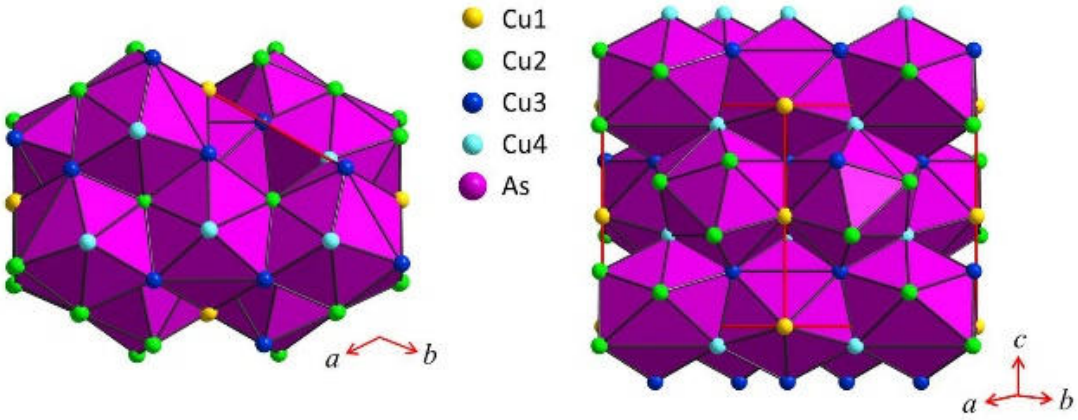

Figure 25. Sketch of the crystal structure of Cu3As where the coordination polyhedra around As atoms As@Cu11 are highlighted.

5.5 Transport/physical property measurements

5.5.1 $Cu_{9-x}(As,Sb)_3$: (sample C7)

Electrical resistivity as a function of T has been measured between 10-300 K. Overall, the compound shows metallic behaviour; however, with an anomalous (heavy-fermions like) behaviour between 300-180 K. The magnetisation as a function of the applied magnetic field *H* shows diamagnetism (**Figures 26** and **27**).

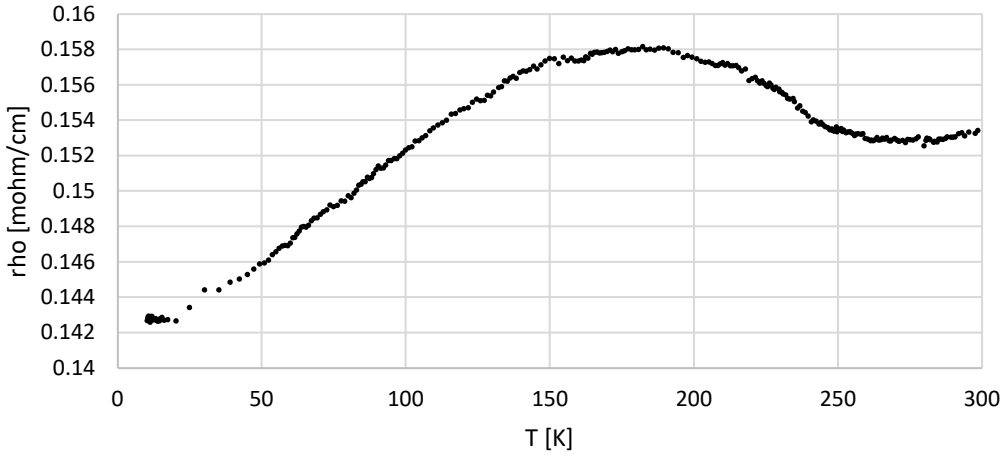

Figure 26. $Cu_{9-x}(As,Sb)_3$: (C7_DTA; $Cu_{72}As_7Sb_{21}$). Electrical resistivity.

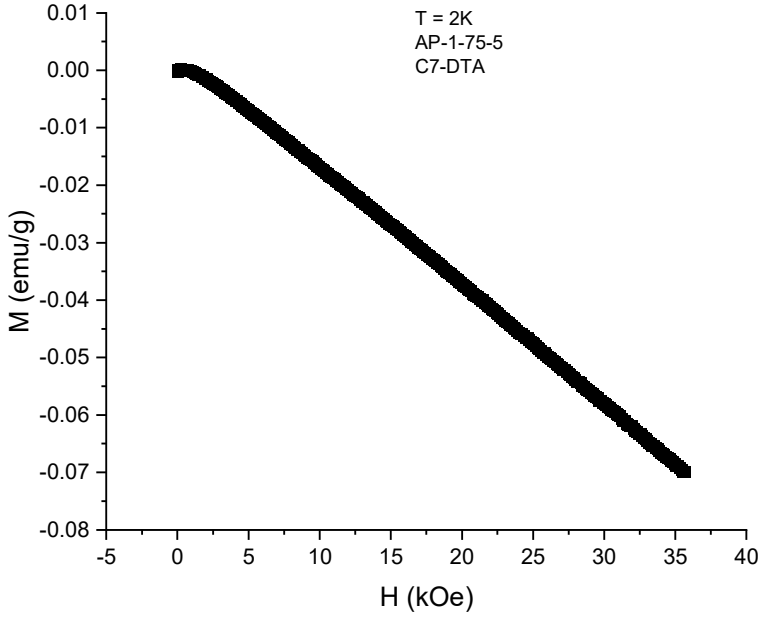

Figure 27. $Cu_{9-x}(As,Sb)_3$: (C7_DTA; $Cu_{72}As_7Sb_{21}$). Magnetization *vs*. magnetic field (H (kOe) measured at T = 2K).

5.5.2 Cu_3As

DTA and XRD do not show any structural change in the Cu_3As compound above room temperature, opposite to what is reported in literature (at about 450-475°C) [22-23]. Instead, we have noted anomalies in the **resistivity measurements** related to a change in structure **(Figure 28**) at low temperature (-80 to 40°C), i.e. at 244 K and 231 K; there is a change of slope noted at around 167 K. The sample shows metallic behaviour with

$$\text{RRR} = \frac{\rho(300\text{K})}{\rho(10\text{K})} = 27$$

Also measurements of **magnetoresistance** (**Figure 29**) were carried out, showing a strong effect caused by the field. Overall, negative values show negative carriers with the **Seebeck** effect (**Figure 30**); we note a discontinuity at 244 K, likely related to a structural 1st order transition. These analyses confirmed a structural 1st order transition (also confirmed by XRD analyses in low temperature on single crystal): the value of *c* triples and, eventually as well, the value of parameter *a* doubles. Further studies are planned to be carried out by synchrotron radiation in low temperature (Grenoble, Alba).

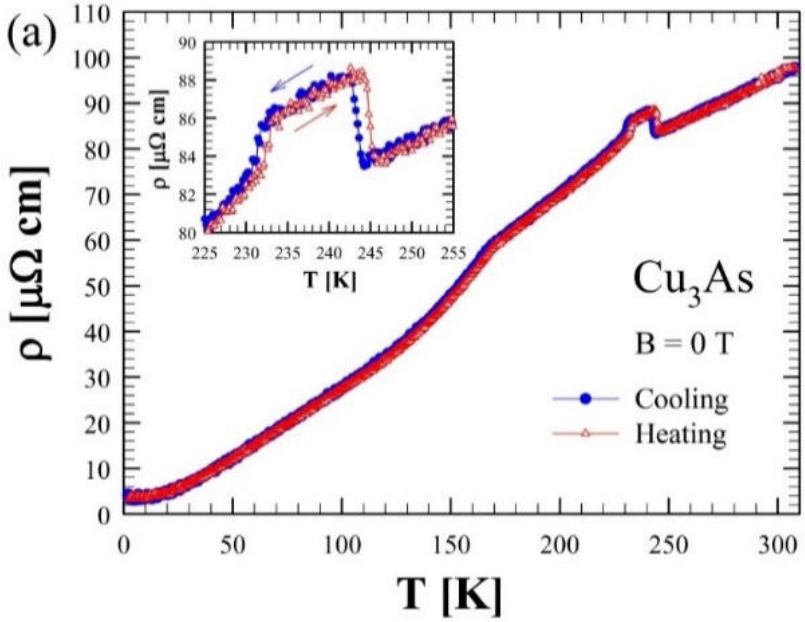

Figure 28. Zero-field electrical resistivity as a function of temperature between 2 and 300 K for Cu_3As measured both on cooling and heating.

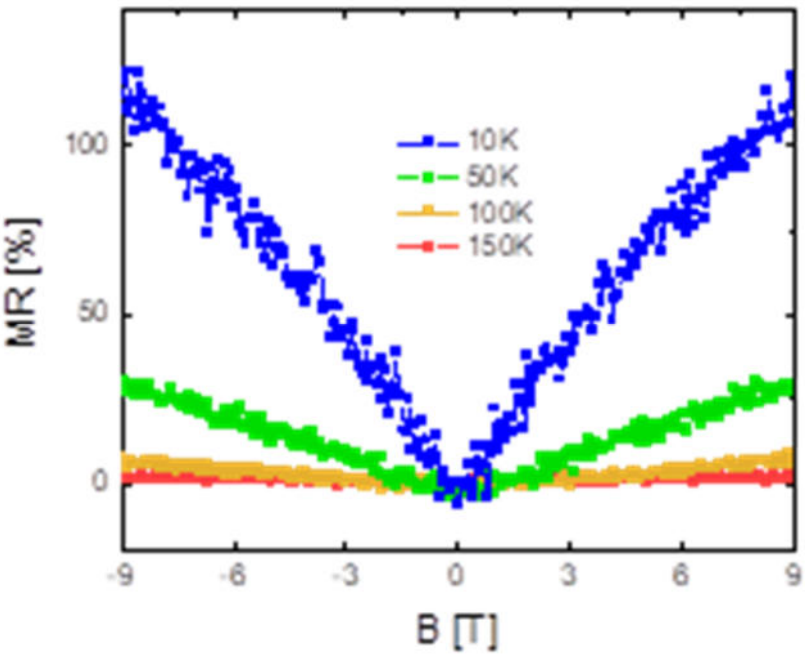

Figure 29. Magnetoresistance as a function of applied magnetic field between 0 and ± 9 T at several temperatures (10 K, 50 K, 100 K and 150 K) for Cu_3As.

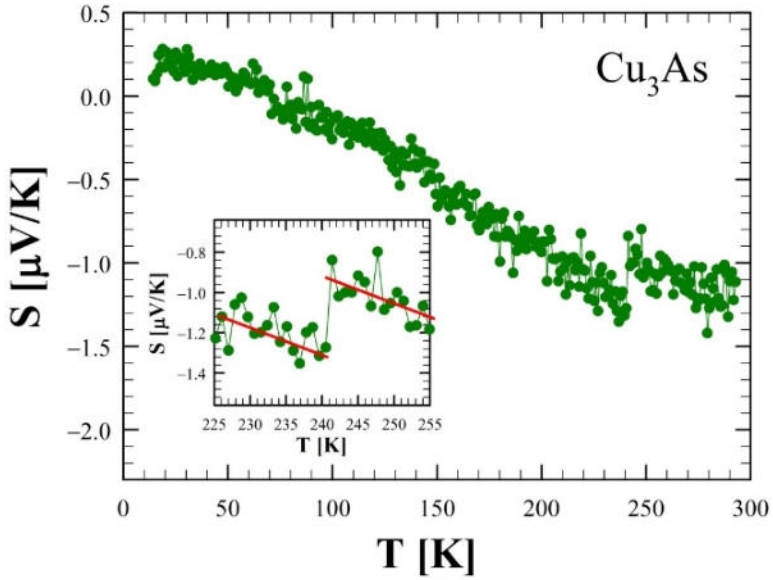

Figure 30. Seebeck-effect. The inset, which shows a magnification of the data between 225 and 255 K, highlights the discontinuity at about 242 K.

6. Conclusions and outlook

Our work on the ternary Cu-As-Sb system revealed severe lacuna in the research up to now performed on both the binary systems As-Sb and Cu-As. For instance, the existence of specific phases (such as Cu_2As, or As_3Sb_7) and their formation is still not clear; other phases were described with wrong type and space group and composition, as in the case of Cu_3As.

This information though is of fundamental importance for the understanding of the Cu-As-Sb system. In part, some of this data could be identified during the course of the PhD

research: it was shown that the **true crystal structure of Cu_3As** is the hexagonal Cu_3P-tpe (*hP*24, *P*63*cm*, No. 185) and not the hexagonal anti HoH_3-type. Moreover, it was also found that Cu_3As does not exist with other modifications at least up to 750 °C, i.e. no HT or LT phases exist, but that and instead present at least one (likely two) structural transition below room temp.

In the ternary Cu-As-Sb system, several new phases were detected and described:

1) $Cu_{3-x}(AsSb)$ of $Cu_{3-x}P$ type, ***hP*24**, space group $P6_3cm$, no. 185 [73.6–77.6 at.% Cu]
2) $Cu_{9-x}(AsSb)_3$ of $Cu_{9.1}(TeSb)_3$-type, ***cP*32**, space group *Pm*-3*n*, no. 223 [71.1-73.5 at.% Cu]
3) $Cu_2(AsSb)$ of Cu_2Sb type, ***tP*6**, space group *P*4/nmm, no. 129 [64.1–67.7 at.% Cu]
4) Sb(As) of As type, ***hR*6**, space group R-3*m* no. 166 [0–1.5 at.% Cu]
5) The structure of the compound **$Cu_{10}(As,Sb)_3$** is not yet identified; however, a strong similarity to the binary compound of $Cu_{10}Sb_3$ confirmed by XRD analyses
6) At least **four different eutectic reactions**, such as: Cu(α) + *cP32*; *tP*6 + *hR*6; *tP*6 + Sb(α). Further analyses will have to confirm the (potential) existence of other eutectics such as Cu(α) + hP24; *cP*32 + *hR*6; *tP*6 + *cP32*; *tP*6 + *hP*24; *hP*24 + Sb(α).

So far, there are no published data neither on transport, nor on other physical property measurements on Cu_3As and Cu_5As_2 or any alloy from the Cu-As-Sb system. However, as part of the PhD-research physical property measurements on Cu_3As were carried out. Low-temperature electric transport measurements showed typical metallic behavior for Cu_3As; the data nicely show clear anomalies in correspondence of the structural changes. From analysis of the Seebeck coefficient as a function of temperature, we have determined a conduction of the n-type. These measurements again probe the first structural transition. The temperature dependence of the magnetic susceptibility, measured for both a single crystal and a polycrystalline sample of Cu_3As, displaying an overall constant diamagnetic response, demonstrated that this compound is a diamagnetic material.

In the binary Cu-As system, both Cu_3As and Cu_5As_2 were studied. It was discovered that **Cu_3As**

1) is of the hexagonal **Cu_3P structure** (LT & HT) (*hP*24, *P*63*cm*, No. 185) [powder and single crystal XRD analyses and structural Rietveld refinement];

2) undergoes two **structural transitions** around 244K (first order) and 231 K [LT XRD and DSC analyses]: parameter *c* triples and, with temperatures below 150 K, parameter *a* doubles;
3) is more **semi-metal** than expected, as its electric resistance is significantly higher than that of Cu metal;
4) shows an unexpectedly **high magnetoresistance**;
5) shows an **anomaly** in form of an electric resistivity plateau, related to parameter *c* and later parameter *a.*

Moreover, DSC analyses on Cu_5As_2 samples showed also on this compound a possible structural transition or decomposition at 310 °C.

Research on both ternary Cu-As-Sn and binary Cu-As systems will continue during the **Marie Skłodowska-Curie IEF Fellowship** [no. 101018804] of Marianne Mödlinger at the University of Genoa from 01/12/2022 – 31/08/2026. Apart from the previous mentioned fundamental data still missing from the binary Cu-As system, both binary and ternary Sb-rich alloys discovered in the Cu-As-Sb system during the PhD-research, such as As_3Sb_7, $Cu_{18}As_9Sb_{73}$ and $Cu_{14}As_6Sb_{80}$ (and eventually other eutectics present in the system) will be studied, in order to build the complete Cu-As-Sb system and not only, as previously planned, from 64-100 at.% Cu.

The results of this PhD research will have an impact in different research fields and applications:

1) **Corrosion Science and Engineering**: Cu-As alloys are known to show high corrosion resistance, which seems to improve with the addition of Sb, especially concerning microbiologically induced corrosion. Their use in highly corrosive environments may be more reliable than current solutions.
2) **Mining Engineering**: Copper ores rich in As, Ni, and Sb (such as sulfosalt minerals) are typically ignored, or, if mined, diluted before processing, which is a very polluting process. Finding new applications of such copper or copper alloys may consequently lead to processes less polluting, as these elements would not need to be removed. Moreover, phase diagrams of the Cu-As-Sb systems are important in the complex copper and lead metallurgy, especially when it comes to speiss formation, as the Cu-

containing speiss has usually a high load of As, Sb, Sn and Ni (speiss is a by-product of copper extraction, consisting mainly of iron and arsenic with trace amounts of other minerals and metals).

3) **Archaeology**: To improve the understanding of adaption, recycling, and final disregard of Cu-As alloys c. 2300 BCE, and to expand the knowledge on prehistoric metal technologies.
4) **Technological applications**: The ternary alloys are completely new and for the first time studied. Their analyses and mechanical, physical and thermal investigations is still ongoing and serves to identify their potential and future use in different applications in various fields. Hence, their future usage is still difficult to define.

7. Acknowledgments

First of all, I would like to thank my supervisor, Prof. Pietro Manfrinetti, for his all-time precious support and help. A warm and special thank you also to Dr. Alessia Provino, State University of New York, Buffalo, USA, for her continuous support on the interpretation of XRD data.

Special thanks goes to the following persons who enabled my through their help and support and cooperation to successfully finish my PhD-thesis: I would like to thank Dr. Cristina Bernini (CNR-SPIN, Genoa) and Dr. Simona Delsante for SEM-EDXS analyses, Dr. Dario Cavallo (DCC, INIGE) for DSC analyses, Dr. Federico Caglieris (CNR-SPIN, Genova) and Dr. Michele Ceccardi (DIFI, UNIGE) for electrical resistivity and Seebeck effect measurements, Dr. Daniele Macciò (DCCI, UNIGE) for DTA analyses, Dr. Marcella Pani (DCCI, UNIGE) for single crystal measurements, and Pavlo Solokha (DCCI, Genoa), for single crystal XRD measurements.

Last but not least: I thank both my children, Helene and Sebastian, for the time I spend working on the PhD and not with them.

8. Publications

I prefer to wait with the publication of the PhD-results until the first few months of my Marie Skłodowska-Curie Fellowship at the University of Genoa (start: 01/12/2022), as the fellowship has a topic closely related and partly overlapping with the PhD-research.

- M. Mödlinger*, A. Provino, P. Solokha, F. Caglieris, M. Ceccardi, D. Macciò, M. Pani, C. Bernini, D. Cavallo, A. Ciccioli, P. Manfrinetti. *Cu_3As: uncommon crystallographic features, low-temperature phase transitions, thermodynamic and physical properties* [MDPI], Open Access. [submitted December 11, 2022].
- M. Mödlinger, P. Solokha, A. Provino, M. Ceccardi, C. Bernini, P. Manfrinetti, *Preliminary studies of single phase $Cu_{12-x}AsSb_3$* [in preparation].

9. References

[1] Mödlinger, M., Sabatini, B. A Re-evaluation of inverse segregation in prehistoric Cu-As objects, Journal of Archaeological Science 74, **2016**, 60–74. DOI 10.1016/j.jas.2016.08.005

[2] Mödlinger, M., Sabatini, B. Bronze Age Caucasian Metalwork: Alloy Choice and Combination. Journal of Archaeological Science: Reports 16, **2017**, 248–257. DOI 10.1016/j.jasrep.2017.10.018

[3] Krause R. Studien zur kupfer- und frühbronzezeitlichen Metallurgie zwischen Karpatenbecken und Ostsee (Rahden, Westfalen, **2003**).

[4] 1Shalev, S., Northover, P. The metallurgy of the Nahal Mishmar Hoard reconsidered, Archaeometry 35(1), **2007**, 35 - 47. DOI 10.1111/j.1475-4754.1993.tb01022.x

[5] Northover, J.P., Exotic alloys in antiquity. Metallurgica Antiqua. Der Anschnitt, Beih. 8, **1998**, 113-121.

[6] Mödlinger, M., Kuijpers, M., Braekmans D., Berger, D. Quantitative comparisons of the color of CuAs, CuSn, CuNi, and CuSb alloys. Journal of Archaeological Science 88, **2017**, 14–23. DOI 10.1016/j.jas.2017.09.001

[7] Dardeniz, G. Why did the use of antimony-bearing alloys in Bronze Age Anatolia fall dormant after the Early Bronze Age?: A Case from Resuloğlu (Çorum, Turkey), PLOS ONE 15(7), **2020**. DOI 10.1371/journal.pone.0234563

[8] Revie, R.W. Uhlig's Corrosion Handbook (3rd edition; Wiley **2011**).

[9] Long, G., Peng, Y., Bradshow, D. A review of copper–arsenic mineral removal from copper concentrates, Minerals Engineering 36-38, **2012**, 179-186. DOI 10.1016/j.mineng.2012.03.032

[10] Yang, J., Bertram, J., Schettgen, T., Heitland, P. Arsenic burden in e-waste recycling workers - A cross-sectional study at the Agbogbloshie e-waste recycling site, Ghana, Chemosphere 261, **2020**, 127712. DOI 10.1016/j.chemosphere.2020.127712

[11] Julander A, Lundgren L, Skare L, et al. Formal recycling of e-waste leads to increased exposure to toxic metals: an occupational exposure study from Sweden. Environment International. **2014** Dec, 73, 243-251. DOI 10.1016/j.envint.2014.07.006

[12] Grund, S. et al. Arsenic and Arsenic Compounds. Ullmann's Encyclopedia of Industrial Chemistry (**2008**).

[13] Brigden, K. et al., Greenpeace Research Laboratories, technical note 10/**2008**.

[14] Mödlinger, M., Macció, D., Sabatini, B., Cziegler, A., Schnideritsch, H. Archaeological Arsenical Bronze: Constantly out-of-equilibrium. Metallurgical and Material Transactions B 49, **2018**, 2505–2513. DOI 10.1007/s11663-018-1322-8

[15] Budd P.D., Ottaway B.S. The Properties of Arsenical Copper Alloys: Implications for the Development of Eneolithic Metallurg. In: Budd P. D. et al. (eds), Archaeological Sciences **1989**, 132–142.

[16] McKerrell H., Tylecote R.F. P. The working of copper-arsenic alloys in the Early Bronze Age and the effect on the determination of provenance. Proceedings of the Prehistoric Society, 38, **1972**, 209-218. DOI 10.1017/S0079497X00012111

[17] Lechtman H. Dirty Copper or Chosen Alloy? A View from the Americas. Journal of Field Archaeology 23(4), **1996**, 477–514.

[18] Böhne C., Technische Beiträge zur Archäologie 2, **1965**, 126–130.

[19] Hansen D., Marryat C., Investigation of the Effects of Impurities on Copper. Part III-The Effect of Arsenic on Copper. Part IV-The Effect of Arsenic Plus Oxygen on Copper, Journal of the Institute of Metals 37, **1927**, 121-168.

[20] Northover J.P. in: Hauptmann A., Pernicka E., Wagner G.A. (eds). Archäometallurgie der Alten Welt, Der Anschnitt Beiheft 7, 111–118 (Bochum **1989**).

[21] Thompson, D.H. and Tracy, A.W., JOM 1/2, **1949**, 100-109.

[22] Subramanian P.R., Laughlin D.E. in: Subramanian P. R. (ed). Phase diagrams of binary copper alloys (Ohio), **1994**, 43–52.

[23] Subramanian P.R., Laughlin D.E. The As−Cu (Arsenic-Copper) system. Bulletin of Alloy Phase Diagrams 9, **1988**, 605–618. DOI 10.1007/BF02881964

[24] Zwicker U., Natural Copper-arsenic Alloys and. Smelted Arsenic Bronzes in Early Metal Production, in: Mohen J.-P. (ed). Découverte du métal II (Paris **1991**), 331–340.

[25] Rosenberg, M., Vija, H., Kahru, A. et al. Rapid in situ assessment of Cu-ion mediated effects and antibacterial efficacy of copper surfaces. Sci Rep 8, 8172 (**2018**). DOI 10.1038/s41598-018-26391-8

[26] Dupont, C.L., Grass, G., Rensing, C. Copper toxicity and the origin of bacterial resistance--new insights and applications. Metallomics 3, **2011**, 1109–1118. DOI 10.1039/c1mt00107h

[27] Hans M, Erbe A, Mathews S, Chen Y, Solioz M, Mücklich F. Role of copper oxides in contact killing of bacteria. Langmuir 29, **2013**, 16160–16166. DOI 10.1021/la404091z

[28] Inkinen J, Mäkinen R, Keinänen-Toivola MM, Nordström K, Ahonen M. Copper as an antibacterial material in different facilities. Lett Appl Microbiol. **2017** Jan; 64(1), 19-26. DOI 10.1111/lam.12680. Epub 2016 Nov 28. PMID: 27718259

[29] Lucey, V. F. The mechanism of dezincification and the effect of arsenic II, Brit Corros J 1(2), **1965**, 53–59.

[30] Lucey, V.F. The mechanism of dezincification and the effect of arsenic I, Brit Corros J 1(1), **1965**, 9-14.

[31] Ahmad, Z. Principles of Corrosion Engineering and Corrosion Control (Butterworth-Heinemann: Oxford, **2006**).

[32] Piccardo, P., Mödlinger, M., Ghiara, G., Campodonico, S., Bongiorno, V. Investigation on a "tentacle-like" corrosion feature on Bronze Age tin-bronze objects. Journal of applied physics A 113/4, **2013**, 1039–1047. DOI 10.1007/s00339-013-7732-1

[33] Ghiara, G., Repetto, L., Piccardo, P. The effect of pseudomonas fluorescens on the corrosion morphology of archaeological tin bronze analogues, JOM 71 (2), **2019**, 779-783. DOI 10.1007/s11837-018-3138-z

[34] Fürtauer, S., Flandorfer, H. A new experimental phase diagram investigation of Cu–Sb, Monatsh Chem 143, **2012**, 1275–1287. DOI 10.1007/s00706-012-0737-1

[35] Massalski T.B. Cu–Sb (copper–antimony). In: Binary alloy phase diagrams, vol 2, 2nd edn. The Materials Information Society, Materials Park, **1990**.

[36] Massalski T.B. As–Sb (arsen–antimony). In: Binary alloy phase diagrams, vol 2, 2nd edn. The Materials Information Society, Materials Park, 1990.

[37] Ugai, Y.A, Samoilov, A.M., Semenova, G.V., Goncharov, E.G. A thermodynamic analysis of the interaction of the antimony-arsenic system components. Zhurnal Fizicheskoi Khimii, 60, **1986**, 25-28.

[38] Villars P., Prince A., Okamoto H. (eds.). Handbook of Ternary Alloy Phase Diagrams. ASM, **1995**.

[39] Koenig, G.A. Über die künstliche Darstellung von Krystallen des Mohawkits, des Domeykits, des Argentodomeykits, des Stibiodomeykits, des Keweenawits und

anderer Arsenide. Zeitschrift für Kristallographie 38 (6), **1903**, 529-543. DOI: 10.1524/zkri.1904.38.1.529

[40] Weil, R., Hocart, R. Simultaneous Synthesis of Cubic and Hexagonal Domeykite from Liquid Mixtures at Ordinary (Atmospheric) Pressures, Comptes Rendus de l'Académie des Sciences 233(1), **1951**, 880-882.

[41] 1Villars, P., Cenzual, K. Pearson's Crystal Data - Crystal Structure Database for Inorganic Compounds (on DVD), Release **2020/2021**, ASM International, Materials Park, OH, USA.

[42] Bolfa, J., Pastant, R., Roubalt, M. Réalisation de la synthèse des arséniures de Cu par frittage, Comptes Rendus de l'Académie des Sciences 230(1), **1950**, 103-104.

[43] Iglesias, J.E., Nowacki, W. Refinement of the crystal structure of a domeykite, a structure related to the A415 type, Zeitschrift für Kristallographie 145, **1977**, 334-345.

[44] Gierlotka, W. – Jendrzejczyk-Handzlik, D. Thermodynamic description of the Cu–Sb binary system, Journal of Alloys and Compounds 484, **2009**, 172–176. DOI 10.1016/j.jallcom.2009.05.056

[45] Yvon, K., Jeitschko, W., Parthé, E. LAZY PULVERIX, a computer program. J. Appl. Crystallogr. 10, **1977,** 73-74.

[46] 1Rodriguez-Carvajal, Recent advances in magnetic structure determination by neutron powder diffraction J. Physica B 192, **1993**, 55-69. DOI 10.1016/0921-4526(93)90108-I

[47] Søtofte, I., Makovicky, E., & Karup-Møller, S. The crystal structure of Cu9.1(1)TeSb3, a stuffed derivative of Cr3Si. Zeitschrift für Kristallographie - Crystalline Materials, 213, **1998**, 282-385.

[48] P. Németh, L. A. J. Garvie, T. Aoki, N. Dubrovinskaia, L. Dubrovinsky, P. R. Buseck, Lonsdaleite is faulted and twinned cubic diamond and does not exist as a discrete material, *Nature Commun*. 5 **2014**, 5447. DOI: 10.1038/ncomms6447

[49] A. V. Kurdyumov, V. F. Britun, V. V. Yarosh, A. I. Danilenko, V. B. Zelyavskii. The influence of the shock compression conditions on the graphite transformations into lonsdaleite and diamond. *J. Superhard. Mater*. 34 **2012,** 19–27. DOI: 10.1073/pnas.83.11.3569

[50] L. Pauling, B. Kamb, A revised set of values of single-bond radii derived from the observed interatomic distances in metals by correction for bond number and resonance energy. *Proc. Natl. Acad. Sci*. USA 83, **1986,** 3569-3571. DOI 10.3103/S1063457612010029